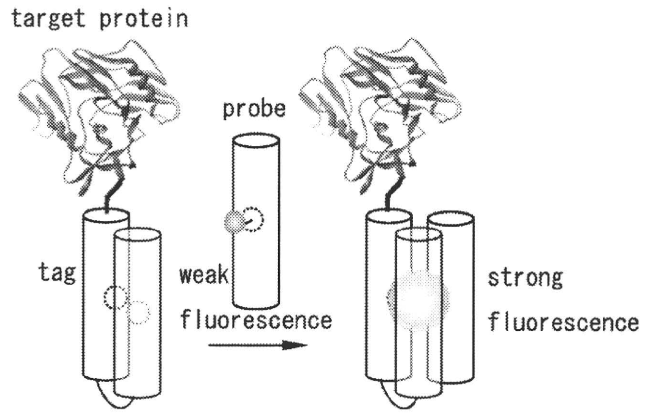

FIGURE 1 Formation of tag-probe pairs with fluorogenic activity based on the artificial leucine zipper peptides, designated as ZIP tag-probe pairs, and their application to the fluorescent imaging of ZIP tag-fused proteins.

cation of recombinant proteins[16] and as anchors for the immobilization of proteins on micro plates.[17] Complementary selectivity and strong binding affinity have prompted application of new tag-probe pairs to the bio-imaging of proteins. Since hydrophobic cores of leucine zipper peptides can be adjusted to form hydrophobic pockets in which small molecules can bind,[18,19] selective binding of environmentally sensitive fluorescent dyes to these pockets inside the leucine zipper assembly might lead to colorimetric changes and enhance their fluorescence intensity. Accordingly, we have developed new tag-probe pairs with fluorogenic activity based on the artificial leucine zipper peptides, designated as ZIP tag-probe pairs, and applied them to the fluorescent imaging of ZIP tag-fused protein on the surface of living cells (see Figure 1).[20]

The design of ZIP tag-probe pairs was based on the crystal structure of an antiparallel coiled-coil trimer of a GCN4 mutant shown in Figure 2.[21] A probe peptide consists of an α-helical peptide in which 4-nitrobenzo-2-oxa-1,3-diazole (NBD), an environmentally sensitive fluorescent dye is imbedded. The NBD is attached to the side chain of the L-α-2,3-diaminopropionic acid residue (Dap(NBD)) at position 13 on the hydrophobic site of the leucine zipper structure. A tag peptide consists of antiparallel 2 α-helical peptides linked via a Gly-Gly-Cys-Gly-Gly loop sequence. Two Leu residues in the tag peptide, located at the positions complementary to the Dap(NBD) residue of the probe peptide, are replaced by Ala so that an adequate hydrophobic pocket is formed when the tag peptide binds to the probe peptide.

In fluorescent titration analysis, the change in the fluorescence spectra of the probe peptide depends largely on the concentration of the tag peptide. The emission spectra derived from NBD showed a 17-fold increase in emission intensity with a concomitant blue shift of the emission maximum from 535 nm to 505 nm (see Figure 3). This spectral change shows that the NBD moiety of the probe peptide is located in the hydrophobic environment inside the 3α-helical peptide bundle structure. The dissociation constant of the probe peptide toward the tag peptide, was estimated by analysis of the fluorescent titration curve with a nonlinear least-squares curve fitting method[22] at 18 n*M*. The tag-probe pair was also applied to the fluorescent imaging of the tag-fused CXCR4 by the probe peptide in the living cells. CXCR4 is a member of a chemokine receptor family, involving seven transmembrane G-protein coupled receptor (7TM-GPCR) families.[23,24] The tag-fused CXCR4, in which the tag is genetically fused to the extracellular N-terminus region of CXCR4, is transiently expressed on the surface of CHO-K1 cells. Sequential labeling experiments of the tag-fused CXCR4 using the probe peptide with the NBD dye and a fluorescent CXCR4 antagonist were performed. In the presence of the excess probe peptide, the labeling of tag-fused CXCR4 using the probe peptide with NBD produced bright green fluorescence on the surface of the cells (see Figure 4).[25] Subsequently, the tag-fused CXCR4 was stained in a red color by the CXCR4 antagonist, tetramethylrhodamine (TAMRA)-appended T140. In this way, a membrane protein CXCR4 can be successfully visualized using the ZIP tag-probe system which this is shown to be a useful fluorescent imaging tool for proteins in living cells. The tag-probe complex consist-

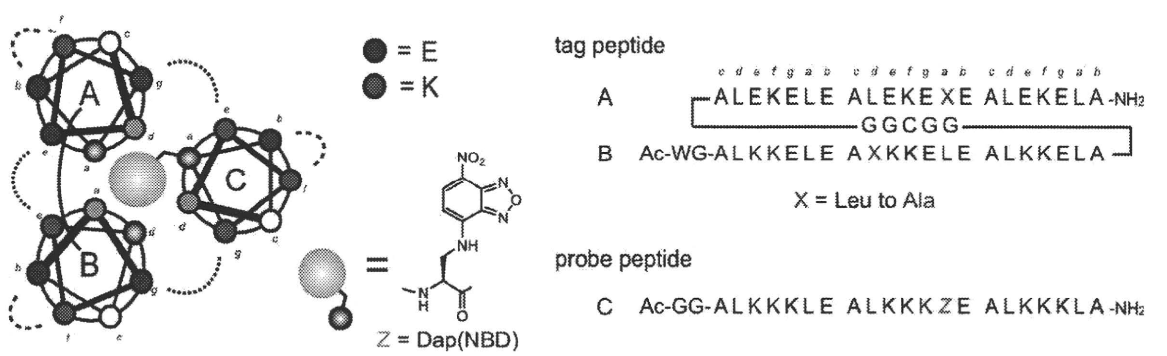

FIGURE 2 Design and structure of ZIP tag-probe pairs.

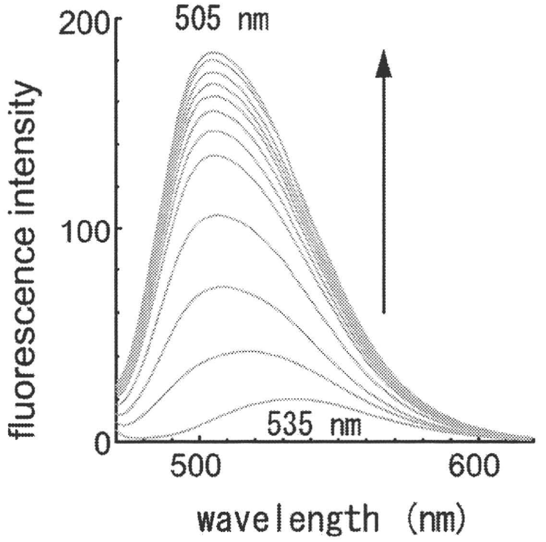

FIGURE 3 Fluorescence spectral change of the probe peptide upon the addition of the tag peptide at 25°C in 50 mM HEPES buffer (pH 7.2, 100 mM NaCl): [probe] = 0.5 μM, [tag] = 0 to 2.0 μM.

ing of the antiparallel 3α-helical peptide bundle structure is formed as a result of the affinity of the tag peptide and the probe peptide. Since this interaction involves noncovalent bonds, introduction of crosslink by a covalent bond might increase chemical and biological stability. Thus, we developed tag-probe pairs, crosslinked by covalent bonds (see Figure 5).

RESULTS AND DISCUSSTION

Crosslinking Reaction of the Tag Peptide With the Probe Peptide

To investigate the optimum length of crosslinkers, three types of probe peptides with linkers of different lengths were synthesized. The original tag peptide has a side-chain thiol group in the Gly-Gly-Cys-Gly-Gly loop structure between antiparallel 2α-helical peptides. At the N-terminus of each probe peptide, 0, 1, or 2 Gly residues were attached as a spacer and an N$^{\alpha}$-chloroacetyl group as a functional group for coupling with the Cys thiol group (see Figure 6). The probe peptides having 0, 1, and 2 Gly residues were designated probe **1**, **2**, and **3**. As control probe peptides, probe peptide **4**, which has no chloroacetyl group, and **5**, which has N$^{\varepsilon}$-chloroacetyl-Lys at the C-terminus, both possessing N$^{\alpha}$-acetyl-Gly, were also prepared. Probe peptides **1-5** were prepared by Fmoc-based solid-phase peptide synthesis.[26] The tag peptide was prepared by native chemical ligation[27,28] of the synthetic C-terminal thioester fragment A and the N-terminal cysteine fragment B, which were divided at the cysteine residue of the loop sequence.[20] Using the probe peptides **1-3**, the crosslinking reactions with the tag peptide, monitored by HPLC,[29] were performed by addition of the tag peptide to the probe peptide (1:1, final 1 μM each) in 50 mM HEPES buffer, pH 7.2 containing 100 mM NaCl at room temperature. The time course of the crosslinking reaction of the probe peptide **2** is shown in Figures 7 and 8a. Peak areas of the tag peptide and the probe peptide **2** with the retention times of $\sim$18 min and 32 min, respectively, decreased in a time-dependent manner, while that of the product of crosslink, the tag-probe **2** complex, with retention time of 28 min, increased. Completion of this reaction was the fastest of the crosslinking reactions, requiring approximately 20 min (Figure 8b). The order of the reaction rate of the probe peptides was **2**, **1**, **3**, and **5** (Figures 8b and 9). Reactions of **1** and **3** were mostly complete in 30 min, and the crosslinking reaction of the tag peptide with the probe peptide **5** failed (see Figure 9). These results suggest that a Gly residue at position 1 is the most suitable spacer and that the chloroacetyl group of the probe peptide and the thiol group of the tag peptide react in a structure-specific manner. In the use of the probe peptides **1-3** to form the tag-probe pairs, the chloroacetyl and thiol groups approach one another prior to the cross-

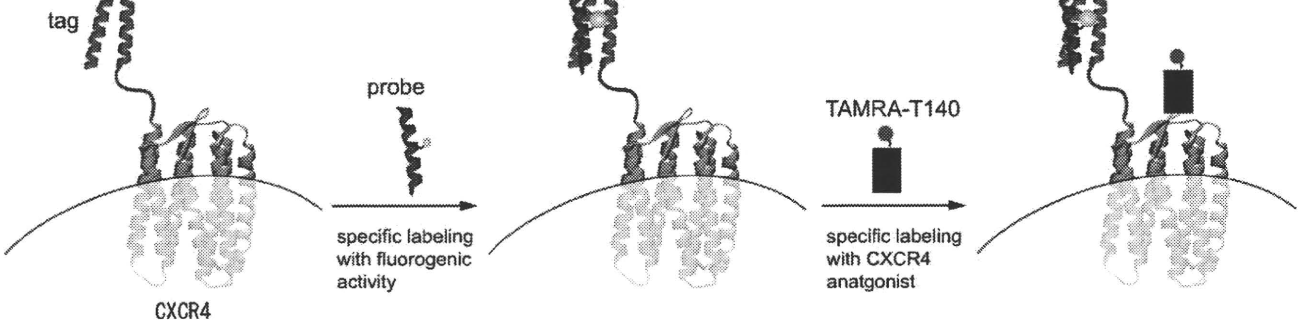

FIGURE 4 Sequential labeling of the tag-fused CXCR4 on the cell surface by the TAMRA-appended CXCR4 antagonist T140 after the labeling by the probe peptide.

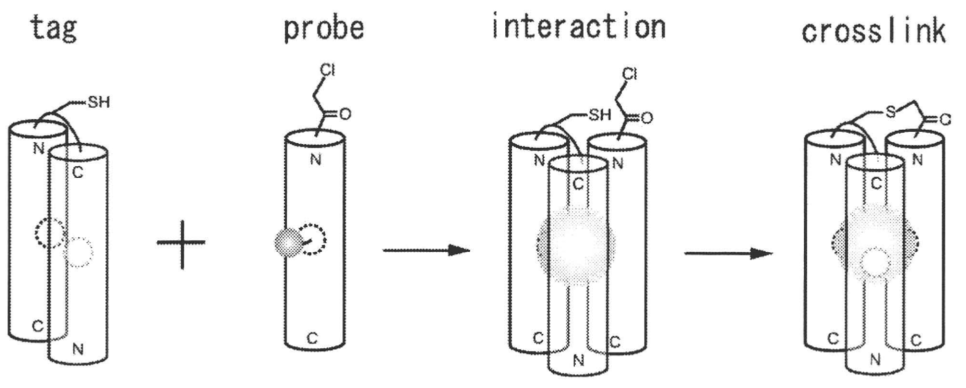

FIGURE 5 Crosslink-type ZIP tag-probe pairs with fluorogenic activity: formation of tag-probe pairs and the subsequent crosslink by a covalent bond.

linking reaction. In the case of the probe peptide **5**, when the tag-probe pair is formed the chloroacetyl and thiol groups are located quite separately on opposite sides and can not interact. All of the crosslink products were purified by RP-HPLC and characterized by ESI-MS.

Fluorescent Titration Analysis

In the fluorescent titration analysis of the addition of the tag peptide to the probe peptide **2**, the fluorescence spectra of **2** changed remarkably, depending on the concentration of the tag peptide. The emission maximum due to the NBD dye showed a significant blue shift from 537 nm to 504 nm with a 22-fold increase in the emission intensity (see Figure 10). Such a spectral change clearly suggests that the NBD moiety of the probe peptide is located in the hydrophobic environment inside the 3α-helical peptide bundle structure, as in noncovalent type formation of the ZIP tag-probe pair.[20] Comparison with the other probe peptides in the fluorescent titration analysis is shown in Figure 10b and Table I. In the use of all of the probe peptides, a similar blue shift of the emission maximum due to the NBD dye from 534–537 nm to 504 nm was observed. The increase of emission intensity, most remarkable in the case of probe peptide **2**, was in the order **2**, **1**, **3**, **4**, and **5**. This suggests that tag-probe **2** pair is most suitable for analytical purposes.

The dissociation constants of the probe peptides **1**, **2**, **3**, **4**, and **5** toward the tag peptide were estimated by analysis using nonlinear least-squares curve fitting[22] as 6.2 n*M*, 6.5 n*M*, 9.0 n*M*, 22 n*M*, and 12 n*M*, respectively (Table I). Thus, in terms of dissociation constant, the probe peptide **1** is comparable to **2**, indicating similar binding affinities, but the hydrophobic environment formed by the interaction of the tag peptide with the probe peptide **2** would appear to be more suitable for the fluorescence emission of the NBD dye.

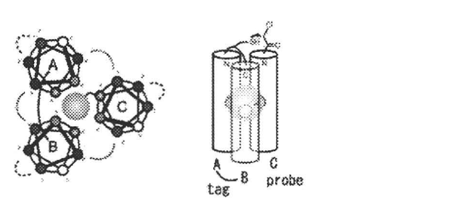

tag fragment A ALEKELE ALEKEAE ALEKELA
GGC/GG
tag fragment B ALKKELE AAKKELE ALKKELA

probe 1 $ClCH_2CO$ ALKKKLE ALKKKZE ALKKKLA
probe 2 $ClCH_2COG$ ALKKKLE ALKKKZE ALKKKLA
probe 3 $ClCH_2COGG$ALKKKLE ALKKKZE ALKKKLA
probe 4 CH_3COG ALKKKLE ALKKKZE ALKKKLA
probe 5 CH_3COG ALKKKLE ALKKKZE ALKKKLAK($COCH_2Cl$)

Z = Dap(NBD)

FIGURE 6 Design and structure of crosslink-type ZIP tag-probe pairs. Probe peptides **1-3** have an N^{α}-chloroacetyl group at the N-terminus. Probe peptides **4** and **5** have an N^{α}-acetyl group at the N-terminus. Probe peptide **5** has N^{ε}-chloroacetyl-Lys at the C-terminus.

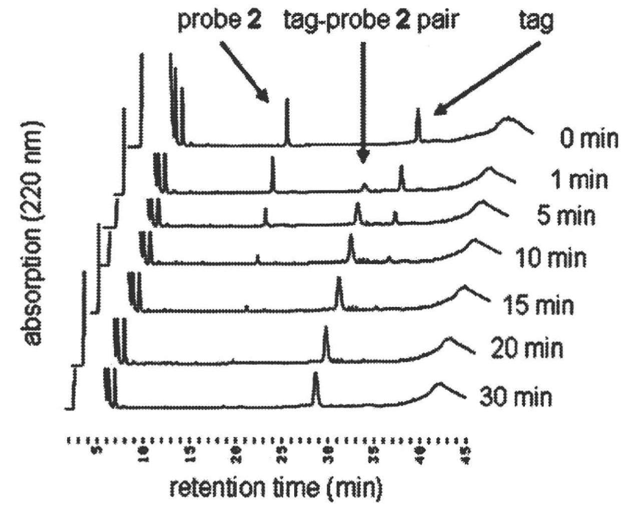

FIGURE 7 HPLC monitoring of the crosslinking reaction of the tag peptide with the probe peptide **2**. The reaction was performed by addition of the tag peptide to the probe peptide **2** (1:1, final 1 μ*M* each) in 50 m*M* HEPES buffer, pH 7.2 containing 100 m*M* NaCl at room temperature.

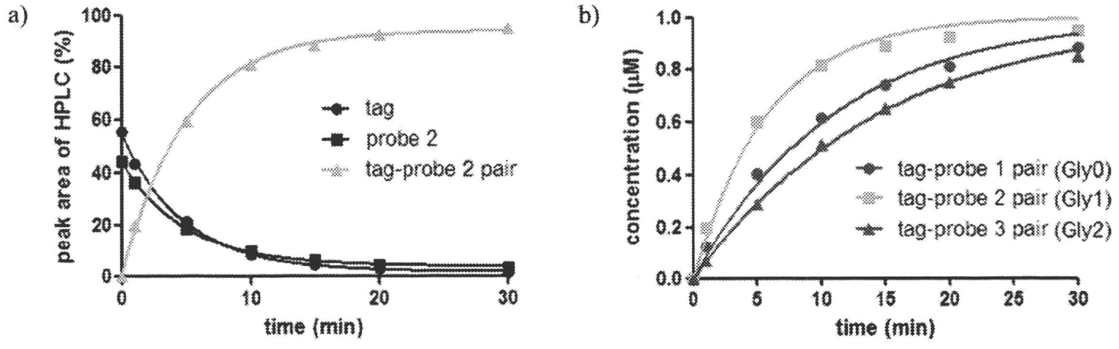

FIGURE 8 The time course of the crosslinking reaction of the tag peptide with the probe peptides. (a) The time course of HPLC peak areas of tag, probe **2** and tag-probe **2** pair, (b) the time course of concentrations of resulting tag-probe **1-3** pairs.

Compared with the noncovalent tag-probe **4** pair, whose dissociation constant is 22 n*M*, the affinities of the covalent type tag-probe **1**, **2**, and **3** pairs are remarkably higher, suggesting that crosslink of tag and probe peptides underlies the increase in affinity. In the tag-probe **5** pair, a similar spectral change was observed, indicating that the NBD dye was located in the hydrophobic pocket, although a covalent bond for crosslink of tag and probe peptides was apparently absent (see Figure 11).

Fluorescence Job's Titration

Fluorescent Job's titration, recording the intensity at 505 nm, was performed to assess the stoichiometry of the tag-probe **2** complex (see Figure 12). The total concentration of the probe peptide **2** and the tag peptide was fixed at 1.0 μM. The concentrations of the tag peptide were 0, 0.2, 0.4, 0.5, 0.6, 0.8, and 1.0 μM. This fluorescence Job's titration experiment clearly indicates that the probe peptide **2** binds to the tag peptide with 1:1 stoichiometry. The result suggests that the tag peptide and the probe peptides **1-3** form a stable 3α-helical leucine zipper structure by binding with 1:1 stoichiometry.

Investigation of Chemical Stability by Fluorescence Analysis

The chemical stability to thermal denaturation of the tag-probe complexes was investigated. Using the complexes of the tag peptide and the probe peptides **1-5**, changes of fluorescence intensity were monitored. The aqueous solution of 1 μM tag-probe complex in 50 m*M* HEPES buffer, pH 7.2 containing 100 m*M* NaCl was prepared, and then the temperature of the solution was gradually increased to 100°C. Fluorescence spectral changes of the tag-probe peptide **2** and **4** pairs, representatives of crosslink pairs and noncrosslink pairs, are shown in Figure 13. In Figure 14 changes of fluorescence intensity of the tag-probe peptide **1-5** pairs are shown. In each of the complexes of the tag peptide with probe peptides **1-5**, a gradual

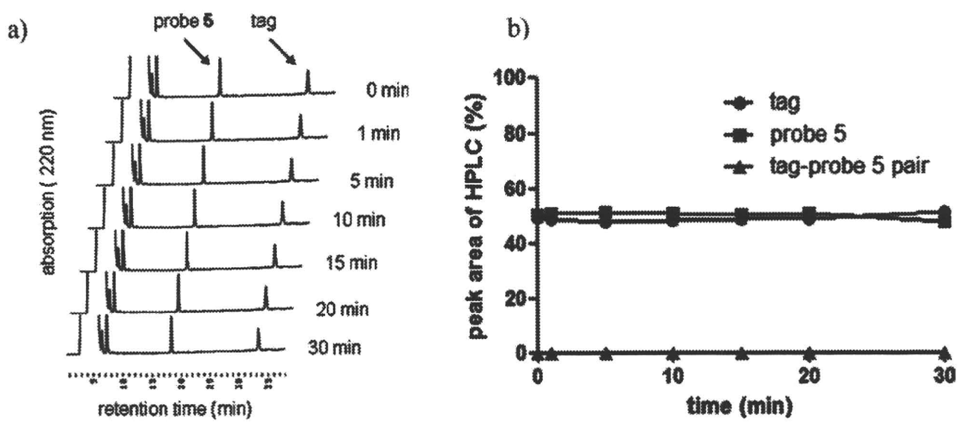

FIGURE 9 (a) HPLC monitoring of the crosslinking reaction of the tag peptide with the probe peptide **5**. The reaction was performed by addition of 1 μM tag peptide to 1 μM probe peptide **5** in 50 m*M* HEPES buffer, pH 7.2 containing 100 m*M* NaCl at room temperature. (b) The time course of HPLC peak areas of tag, probe **5** and tag-probe **5** pair.

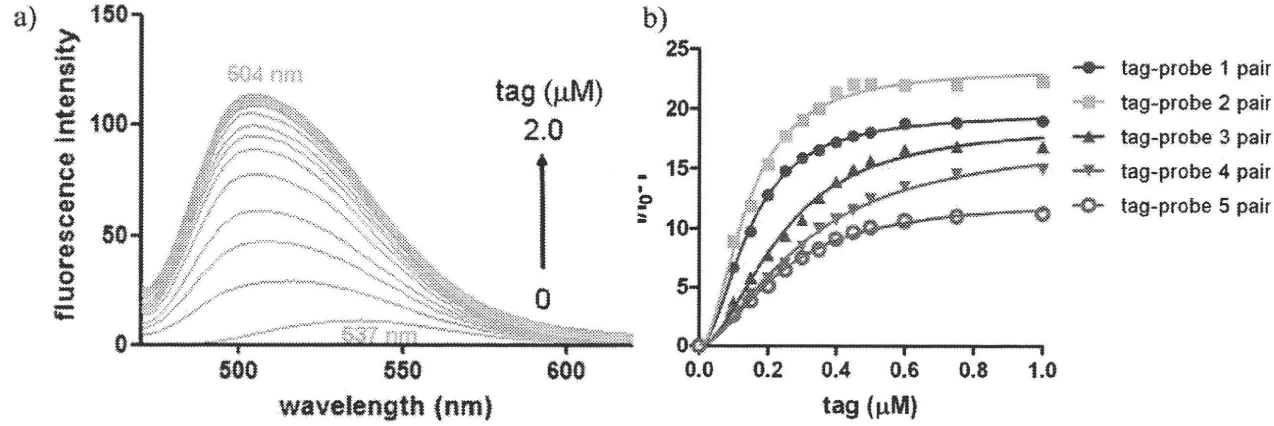

FIGURE 10 (a) Fluorescence spectral change of the probe peptide **2** upon the addition of the tag peptide at 25°C in 50 m*M* HEPES buffer (pH 7.2, 100 m*M* NaCl): [probe] = 0.5 *μM*, [tag] = 0 to 2.0 *μM*. (b) Change of fluorescence intensity of the probe peptides **1-5** upon the addition of the tag peptide for calculation of dissociation constants of tag-probe pairs.

decrease in fluorescence intensity was observed in proportion to the increase of temperature. The complexes of the tag peptide and the probe peptides **1-3** were more stable than those of **4** and **5**, which were completely denatured at 100°C, but the complexes using **1-3** were not denatured, possibly due to the crosslinking. The melting temperatures of the complexes using **1-3** were above 69°C, whereas those of the complexes involving **4** and **5** were below 56°C.

The possibility that this thermal denaturation is reversible was next investigated. The pairs of tag-probe **2** and tag-probe **4** were adopted as representative of crosslink pairs and non-crosslink pairs, respectively. After denaturing the tag-probe **2** pair at 100°C, the temperature of the solution was gradually decreased (Figure 15a). In proportion to the decrease of temperature, a gradual increase in fluorescence intensity of probe **2** was observed, resulting finally in complete recovery of the original fluorescence intensity. In contrast, while a gradual increase in fluorescence intensity, proportionate to a decrease in temperature, was also observed after the thermal denaturation at 100°C of tag-probe pair **4**, the fluorescence intensity recovered only to approximately half of its original level (Figure 15b). These results suggest that the crosslinking of tag and probe peptides is critical for complete reversibility of the fluorescence emission.

Table I Results of Fluorescence Titration of Tag-Probe Pairs

	Fluorescence Wavelength of Emission Maximum (nm)	I_{max}/I_0 (Fold)	Dissociation Constant (n*M*)[a]
Tag-probe **1** pair	537–504	19	6.2
Tag-probe **2** pair	537–504	23	6.5
Tag-probe **3** pair	535–504	17	9.0
Tag-probe **4** pair	534–504	15	22
Tag-probe **5** pair	534–504	11	12

[a] Measurement conditions: 50 m*M* HEPES buffer solution (pH 7.2, 100 m*M* NaCl), at 25°C, [probe] = 0.5 *μM*.

Investigation of Chemical Stability by Circular Dichroism

The chemical stability of the tag-probe complexes to thermal denaturation was investigated by circular dichroism (CD). The CD spectra showed that all of the tag-probe **1-4** complexes form α-helical structures. The CD spectrum of the tag-probe **2** complex had the strongest double minima at 207 and 222 nm, while the spectrum of the non-covalent type tag-probe **4** complex showed the weakest double minima among the four complexes (see Figure 16). This result sug-

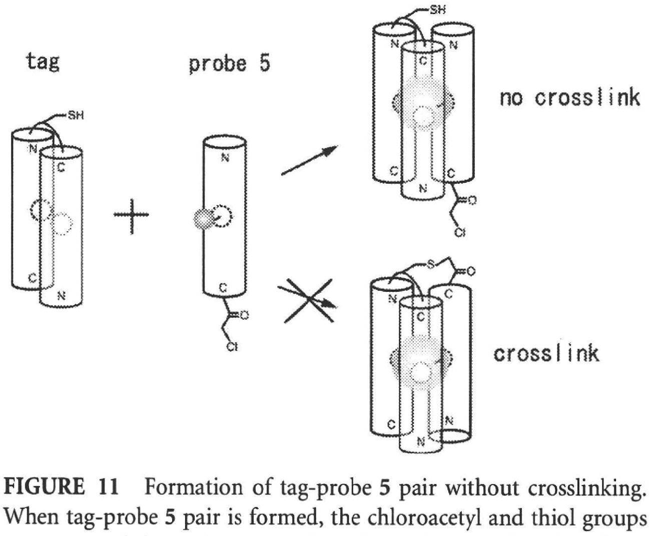

FIGURE 11 Formation of tag-probe **5** pair without crosslinking. When tag-probe **5** pair is formed, the chloroacetyl and thiol groups are separated, located on opposite sides and no covalent bond can form between them.

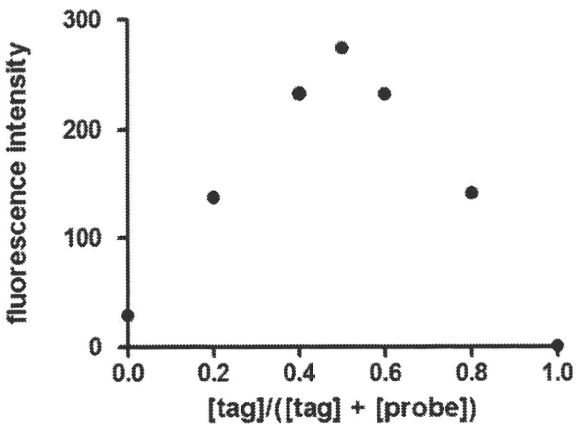

FIGURE 12 Fluorescence Job's titration between the probe peptide **2** and the tag peptide, [probe **2**] + [tag] = 1.0 μM, in 50 mM HEPES buffer (pH 7.2, 100 mM NaCl) at 25°C.

gests that crosslinking of the tag and probe peptides is essential for the α-helical structures. Changes in $[\theta]$ at 222 nm in aqueous solution of 1 μM tag-probe pair in 50 mM Tris-HCl buffer, pH 7.2 containing 100 mM NaCl were monitored, and the temperature of the solution was gradually increased to 94°C (Figure 17a). In all the tag-probe **1-4** pairs, a gradual increase in values of $[\theta]$ at 222 nm was observed in proportion to the increase in temperature. Tag-probe **4** pair, in particular, showed a remarkable increase in values of $[\theta]$ at 222 nm, suggesting that the α-helical structures were largely collapsed. Judging by the changes of $[\theta]$ at 222 nm, the α-helical structures of tag-probe **1-3** pairs survived better than those of tag-probe **4** pair, possibly due to the crosslinking. Next, whether the above α-helical structures can be reversibly recovered was investigated (Figure 17b). The pairs of the tag peptide and the probe peptides **2** and **4** were adopted as representatives of crosslink pairs and noncrosslink pairs, respectively. After denaturing the tag-probe **2** and **4** pairs at 94°C,

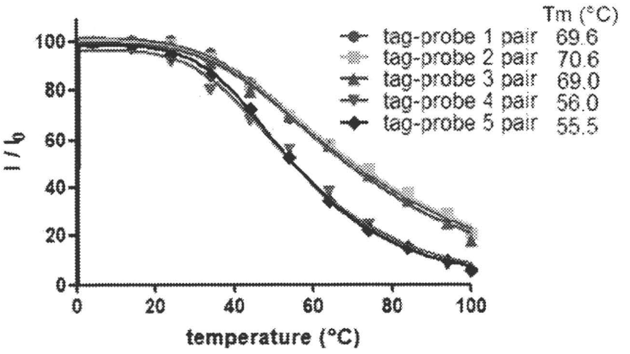

FIGURE 14 Change of fluorescence intensity of tag-probe **1-5** pairs from 4°C to 100°C in 50 mM HEPES buffer (pH 7.2, 100 mM NaCl): [tag-probe pair] = 0.5 μM. Values of melting temperature (T_m) of tag-probe peptide **1-5** pairs are shown.

the temperature of the solution was gradually decreased., Gradual decreases in values of $[\theta]$ at 222 nm in proportion to the decrease of temperature were observed with both pairs. In the case of the tag-probe **2** pair the value of $[\theta]$ at 222 nm was finally nearly completely recovered but with the tag-probe **4** pair $[\theta]$ was not reduced to its original value, suggesting that the crosslink of tag and probe peptides is indispensable for complete reversibility of the α-helical structures.

CONCLUSION

The novel tag-probe pairs based on leucine zipper peptides, in which the thiol group of the Cys residue of the tag peptide and the chloroacetyl group of the probe peptide were crosslinked, have been studied. They were found to have significant fluorogenic activity, mediated by the binding of the tag peptide to the probe peptide as the noncrosslink-type pairs. Compared with noncrosslinked tag-probe pairs, those that are crosslinked were shown to have some advantages in terms of fluorescence

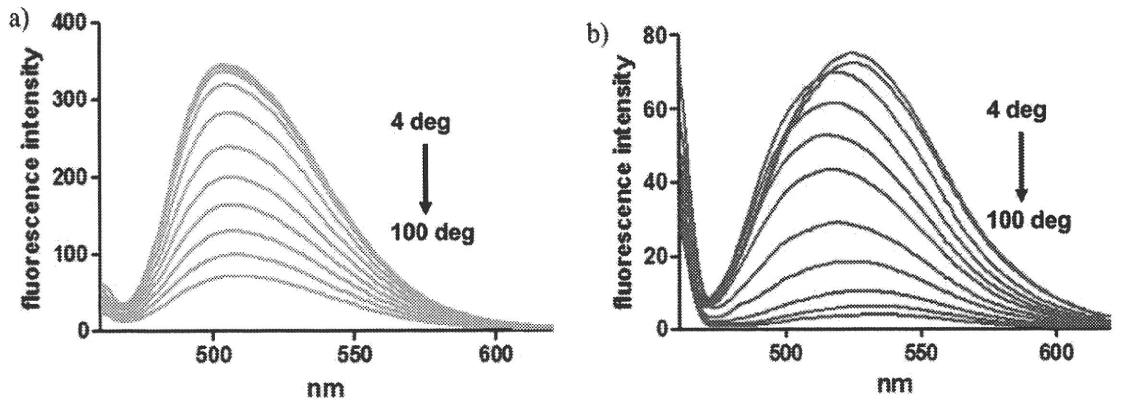

FIGURE 13 Fluorescence spectral change of tag-probe pairs from 4°C to 100°C in 50 mM HEPES buffer (pH7.2, 100 mM NaCl): [tag-probe pair] = 0.5 μM. (a) tag-probe **2** pair, (b) tag-probe **4** pair.

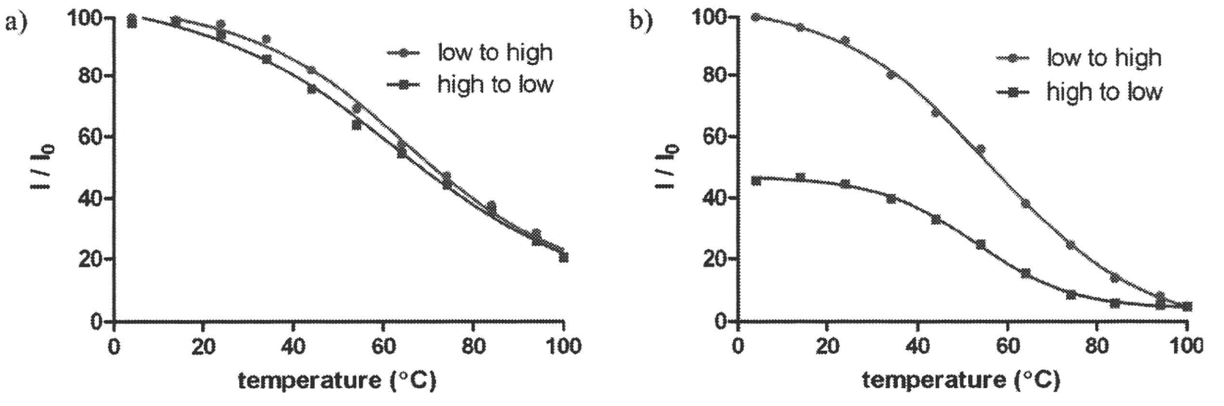

FIGURE 15 Change of fluorescence intensity of tag-probe pairs from 4°C to 100°C (low to high) and from 100°C to 4°C (high to low) in 50 m*M* HEPES buffer (pH 7.2, 100 m*M* NaCl): [tag-probe pair] = 0.5 μM. (a) tag-probe **2** pair, (b) tag-probe **4** pair.

response, binding affinity, and chemical stability. As a spacer between the N^{α}-chloroacetyl group and the original probe sequence, a single Gly residue was superior to 0 or 2 Gly residues. Thus, the probe peptide **2**, having the 1 Gly spacer, binds more rapidly to the tag peptide than the probe peptides **1** and **3**, with 0 and 2 Gly spacers, respectively. Both the previous noncrosslink-type and the present crosslink-type ZIP tag-probe pairs might facilitate the real-time imaging of target proteins without removal of excess probe molecules. Thus, the crosslink-type ZIP tag-probe pairs should be highly useful and valuable for studies of imaging of proteins in living cells.

EXPERIMENTAL PROCEDURES

General

HPLC was carried out on a reversed phase column with a LaChrom Elite HTA system (Hitachi). Matrix-assisted laser desorption/ionization time-of-flight mass spectrometry (MALDI-TOF-MS) was recorded on a Voyager DE-STR (Applied Biosciences) mass spectrometer. 3,5-dimethoxy-4-hydroxycinnamic acid was used as the matrix.

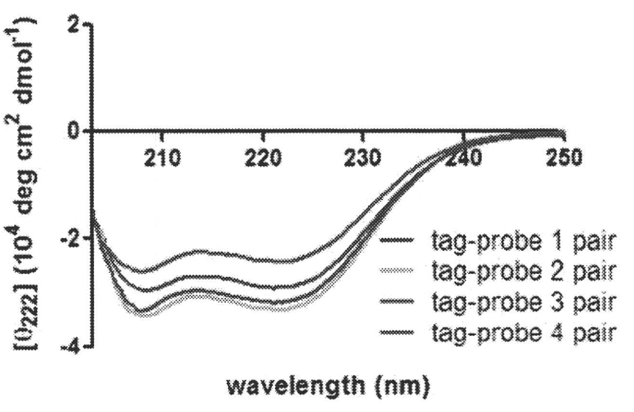

FIGURE 16 CD spectra of tag-probe pairs at 24°C in 50 m*M* Tris-HCl buffer (pH7.2, 100 m*M* NaCl): [tag-probe pair] = 1 μM. Tag-probe peptide **1** pair (blue), tag-probe peptide **2** pair (green), tag-probe peptide **3** pair (red) and tag-probe peptide **4** pair (magenta).

Peptide Synthesis

Probe peptides **1-5** were synthesized by the Fmoc-based solid-phase method.[26] The tag peptide was prepared previously.[20] All peptides were purified by RP-HPLC and identified by MALDI-TOF-MS. Fmoc-protected amino acids and reagents for peptide synthesis were purchased from Novabiochem, Kokusan Chemical Co., Ltd. and Watanabe Chemical Industries, Ltd. Fmoc-Dap(NBD)-OH was synthesized as previously reported.[30] The probe peptides **1-5** were synthesized using NovaSyn TGR resin on a 0.1 mmol scale. All peptides were synthesized by stepwise elongation techniques of Fmoc-protected amino acids on the resin. The coupling reactions were performed using 5.0 equiv. of Fmoc-protected amino acid, 5.0 equiv. of diiopropylcarbodiimide (DIPCI) and 5.0 equiv. of 1-hydroxybenzotriazole monohydrate ($HOBt \cdot H_2O$) in DMF (5.0 mL). N-Terminal amino groups of the probe peptides **1-3** were chloroacetylated with chloroacetic acid, DIPCI and HOBt (5.0 equiv. each) in DMF (5.0 mL). N-Terminal amino groups of the probe peptides **4** and **5** were acetylated with acetic anhydride-DMF (1:4, v/v) (5.0 mL). In the synthesis of the probe peptide **5**, Fmoc-Lys(Mtt)-OH (Mtt = 4-methyltrityl) was coupled as the C-terminal Fmoc-protected amino acid. After construction of the protected peptide **5** resin and N-terminal acetylation, the peptide **5** resin was treated by dichloromethane-triisopropylsilane-TFA (94:5:1, v/v) (2.0 mL) for 1 min, and this treatment was repeated 11 times,[31] followed by N^{ε}-chloroacetylation with chloroacetic acid, DIPCI and HOBt (5.0 equiv. each) in DMF (5.0 mL). Cleavage and side chain deprotection of the probe peptides **1-5** was carried out with 10 mL of TFA in the presence of 0.25 mL of *m*-cresol, 0.75 mL of thioanisole, and 0.75 mL of 1,2-ethanedithiol as scavenger, by stirring for 1.5 h. After filtra-

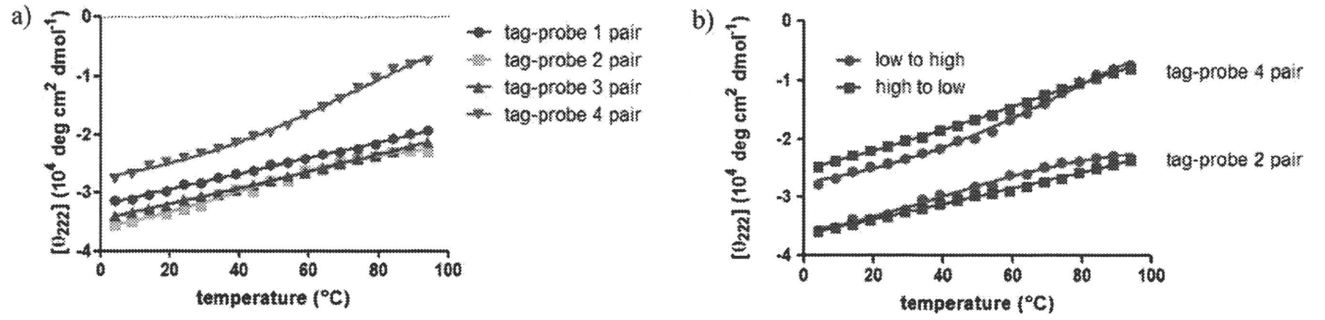

FIGURE 17 (a) Change of values of $[\theta]$ at 222 nm of tag-probe pairs from 4°C to 94°C in 50 m*M* Tris-HCl buffer (pH 7.2, 100 m*M* NaCl): [tag-probe pair] = 1 μM. Tag-probe 1 pair (blue), tag-probe **2** pair (green), tag-probe **3** pair (red) and tag-probe **4** pair (magenta). (b) Change of values of $[\theta]$ at 222 nm of tag-probe **2** and **4** pairs from 4°C to 94°C (low to high) (red) and from 94°C to 4°C (high to low) (blue) in 50 m*M* Tris-HCl buffer (pH 7.2, 100 m*M* NaCl).

tion, the reaction mixture was concentrated under reduced condition, and crude peptides were precipitated in cooled diethyl ether. All crude peptides were purified by RP-HPLC (column, YMC-Pack ODS-A, 10ϕ × 250 mm). The HPLC solvents employed were water containing 0.1% TFA (solvent A) and acetonitrile containing 0.1% TFA (solvent B). The probe peptides **1-5** was purified using a 23%–38% linear gradient of solvent B over 30 min. All purified peptides were identified by MALDI-TOF-MS. All peptides were obtained as TFA salts after lyophilization. Probe peptide **1**, yield 21%, *m/z* 2603.1, calcd 2603.5 $[M + H]^+$. Probe peptide **2**, yield 18%, *m/z* 2661.1, calcd 2660.6 $[M + H]^+$. Probe peptide **3**, yield 23%, *m/z* 2717.1, calcd 2717.6 $[M + H]^+$. Probe peptide **4**, yield 26%, *m/z* 2627.0, calcd 2626.6 $[M + H]^+$. Probe peptide **5**, yield 7%, *m/z* 2773.8, calcd 2773.7 $[M + H]^+$.

Crosslinking Reaction

The probe peptide (16 nmol) and tag peptide (16 nmol) were dissolved in 50 m*M* HEPES buffer, pH 7.2 containing 100 m*M* NaCl (16 mL), and incubated at room temperature in an N_2 atmosphere. At intervals (0, 1, 5, 10, 15, 20, and 30 min), an aliquot (1.6 mL) was sampled and 10% aqueous AcOH (0.4 mL) was added to the aliquot. The reaction was traced by HPLC using a 20%–50% linear gradient of solvent B over 30 min. HPLC peaks of the starting compounds and the generated products were identified by MALDI-TOF-MS: tag-probe peptide **1**, *m/z* 7880.4, calcd 7877.2 $[M + H]^+$. Tag-probe peptide **2**, *m/z* 7935.7, calcd 7934.2 $[M + H]^+$. Tag-probe peptide **3**, *m/z* 7993.8, calcd 7991.3 $[M + H]^+$. The amounts of the starting compounds and the generated products were quantified from the peak areas.

Fluorescence Titration Analysis

Fluorescence spectra were recorded on a JASCO FP-750 spectrometer using a quartz cell. A stock solution of the probe peptide was diluted with 50 m*M* HEPES buffer solution (pH 7.2, 100 m*M* NaCl) to prepare the solution with a final concentration (0.5 μM). The corresponding tag peptide solution was added dropwise to a 0.5 μM of the probe peptide solution and the fluorescence spectra ($\lambda_{ex} = 456$ nm) were measured at 25°C. An average value of three measurements was plotted as each point. Fluorescent titration curves ($\lambda_{em} =$ 537 nm for probe **1** and **2**, 535 nm for probe **3**, and 534 nm for probe **4** and **5**) were analyzed with a nonlinear least-squares curve-fitting method to evaluate K_d values. For measurements of thermal denaturation, fluorescence spectra were recorded every 10°C from 4°C to 100°C after 10-min incubation of tag-probe pairs at each temperature. For measurements in thermal changes from high to low temperature, after 1-h incubation of tag-probe pairs at 100°C, fluorescence spectra were recorded every 10°C until 4°C. Tm values were estimated by a nonlinear least-squares curve-fitting method using GraphPad Prism 5 (MDF Co., Ltd.).

Fluorescence Job's Titration

The fluorescent intensity at 505 nm was recorded on a JASCO FP-750 spectrometer using a quartz cell in 50 m*M* HEPES buffer (pH 7.2, 100 m*M* NaCl) at 25°C. The total concentration of the probe peptide and the tag peptide was fixed at 1.0 μM. The concentrations of the tag peptide were 0, 0.2, 0.4, 0.5, 0.6, 0.8, and 1.0 μM. This fluorescence Job's titration experiment clearly indicates that the probe peptide binds to the tag peptide in a 1:1 stoichiometry.

CD Study

CD were recorded on a J-720WI spectropolarimeter using a quartz cell with 0.1 cm pathlength at 25°C. The stock solutions of tag-probe complexes were prepared and diluted with 50 m*M* Tris-HCl buffer solution (pH 7.2, 100 m*M* NaCl) to prepare the solutions of a final concentration (1.0 μM). Each spectrum shows an average value of three measurements. For measurements of thermal denaturation, CD spectra were recorded every 5°C from 4°C to 94°C after 10-min incubation of tag-probe pairs at each temperature. For measurements in thermal changes from high to low temperature, after 1-h incubation of tag-probe pairs at 94°C, CD spectra were recorded every 5°C until 4°C.

The authors deeply thank Prof. K. Akiyoshi (Tokyo Medical and Dental Univ.) for allowing access to a CD spectropolarimeter.

REFERENCES

1. Terpe, K. Appl Microbiol Biotechnol 2003, 60, 523–533.
2. Hedhammar, M.; Gräslund, T.; Hober, S. Chem Eng Technol 2005, 28, 1315–1325.
3. Guignet, E. G.; Hovius, R.; Vogel, H. Nat Biotechnol 2004, 22, 440–444.
4. Goldsmith, C. R.; Jaworski, J.; Sheng, M.; Lippard, S. J. J Am Chem Soc 2006, 128, 418–419.
5. Hauser, C. T.; Tsien, R. Y. Proc Natl Acad Sci USA 2007, 104, 3693–3697.
6. Griffin, B. A.; Adams, S. R.; Tsien, R. Y. Science 1998, 281, 269–272.
7. Gaietta, G.; Deerinck, T. J.; Adams, S. R.; Bouwer, J.; Tour, O.; Laird, D. W.; Sosinsky, G. E.; Tsien, R. Y.; Ellisman, M. H. Science 2002, 296, 503–507.
8. Marks, K. M.; Rosinov, M.; Nolan, G. P. Chem Biol 2004, 11, 347–356.
9. Ojida, A.; Honda, K.; Shinmi, D.; Kiyonaka, S.; Mori, Y.; Hamachi, I. J Am Chem Soc 2006, 128, 10452–10459.
10. Chen, I.; Choi, Y.-A.; Ting, A. Y. J Am Chem Soc 2007, 129, 6619–6625.
11. O'Hare, H. M.; Johnsson, K.; Gautier, A. Curr Opin Struct Biol 2007, 17, 488–494.
12. Keppler, A.; Gendreizig, S.; Gronemeyer, T.; Pick, H.; Johnsson, K. Nat Biotechnol 2003, 21, 86–89.
13. Gautier, A.; Juillerat, A.; Heinis, C.; Correa, I. R., Jr.; Kindermann, M.; Beaufils, F.; Johnsson, K. Chem Biol 2008, 15, 128–136.
14. Yin, J.; Liu, F.; Li, X.; Walsh, C. T. J Am Chem Soc 2004, 126, 7754–7755.
15. Los, G. V.; Darzins, A.; Karassina, N.; Zimprich, C.; Learish, R.; McDougall, M. G.; Encell, L. P.; Friedman-Ohana, R.; Wood, M.; Vidurgiris, G.; Zimmerman, K.; Otto, P.; Klaubert, D. H.; Wood, K. V. Promega Cell Notes 2005, 11, 2–6.
16. Tripet, B.; Yu, L.; Bautista D. L.; Wong, W. Y.; Irvin, R. T.; Hodges, R. S. Protein Eng 1996, 9, 1029–1042.
17. Zhang, K.; Diehl, M. R.; Tirrell, D. A. J Am Chem Soc 2005, 127, 10136–10137.
18. Obataya, I.; Sakamoto, S.; Ueno, A.; Mihara, H. Biopolymers 2001, 59, 65–71.
19. Yadav, M. K.; Redman, J. E.; Leman, L. J.; Alvarez-Gutie'rrez, J. M.; Zhang, Y.; Stout, C. D.; Ghadiri, M. R. Biochemistry 2005, 44, 9723–9732.
20. Tsutsumi, H.; Nomura, W.; Abe, S.; Mino, T.; Masuda, A.; Ohashi, N.; Tanaka, T.; Ohba, K.; Yamamoto, N.; Akiyoshi, K.; Tamamura, H. Angew Chem Int Ed 2009, 48, 9164–9166.
21. Lovejoy, B.; Choe, S.; Cascio, D.; McRorie, D. K.; DeGrado, W. F.; Eisenberg, D. Science 1993, 259, 1288–1293.
22. Kuwabara, T.; Nakamura, A.; Ueno, A.; Toda, F. J Phys Chem 1994, 98, 6297–6303.
23. Ward, S. G.; Westwick, J. Biochem J 1998, 333, 457–470.
24. Tamamura, H.; Tsutsumi, H.; Nomura, W.; Tanaka, T.; Fujii, N. Exp Opin Drug Disc 2008, 3, 1155–1166.
25. Nomura, W.; Tanabe, Y.; Tsutsumi, H.; Tanaka, T.; Ohba, K.; Yamamoto, N.; Tamamura, H. Bioconjugate Chem 2008, 19, 1917–1920.
26. Chan, W. C.; White, P. D. In Fmoc Solid Phase Peptide Synthesis: A Practical Approach; Chan, W. C.; White, P. D., Eds.; Oxford University Press: New York, 2000; pp 41–76.
27. Dawson, P. E.; Muir, T.W.; Clark-Lewis, I.; Kent, S. B. H. Science 1994, 266, 776–779.
28. Muir, T. W.; Kent, S. B. H. Annu Rev Biochem 2000, 69, 923–960.
29. Nonaka, H.; Tsukiji, S.; Ojida, A.; Hamachi, I. J Am Chem Soc 2007, 129, 15777–15779.
30. Kamoto, M.; Umezawa, N.; Kato, N.; Higuchi, T. Chem Eur J 2008, 14, 8004–8012.
31. Bourel, L.; Carion, O.; Gras-Masse, H.; Melnyk, O. J Peptide Sci 2000, 6, 264–270.

Supplemental Material can be found at:
http://www.jbc.org/content/suppl/2010/06/07/M110.114256.DC1.html

Author's Choice

THE JOURNAL OF BIOLOGICAL CHEMISTRY VOL. 285, NO. 33, pp. 25185–25195, August 13, 2010

Uncoating of Human Immunodeficiency Virus Type 1 Requires Prolyl Isomerase Pin1*

Received for publication, February 16, 2010, and in revised form, May 26, 2010 Published, JBC Papers in Press, June 7, 2010, DOI 10.1074/jbc.M110.114256

Shogo Misumi[‡1,2], Mutsumi Inoue[‡1,3], Takeo Dochi[‡], Naoki Kishimoto[‡], Naomi Hasegawa[‡], Nobutoki Takamune[‡], and Shozo Shoji[‡§]

From the [‡]Department of Pharmaceutical Biochemistry, Faculty of Medical and Pharmaceutical Sciences, Kumamoto University, Kumamoto 862-0973, Japan and [§]Kumamoto Health Science University, Kumamoto 861-5598, Japan

The process by which the human immunodeficiency virus type 1 (HIV-1) conical core dissociates is called uncoating, but not much is known about this process. Here, we show that the uncoating process requires the interaction of the capsid (CA) protein with the peptidyl-prolyl isomerase Pin1 that specifically recognizes the phosphorylated serine/threonine residue followed by proline. We found that the HIV-1 core is composed of some isoforms of the CA protein with different isoelectric points, and one isoform is preferentially phosphorylated in the Ser^{16}-Pro^{17} motif. The mutant virus S16A/P17A shows a severely attenuated HIV-1 replication and an impaired reverse transcription. The S16A/P17A change increased the amount of particulate CA cores in the cytosol of target cells and correlated with the restriction of HIV-1 infection. Glutathione *S*-transferase pulldown assays demonstrated a direct interaction between Pin1 and the HIV-1 core via the Ser^{16}-Pro^{17} motif. Suppression of Pin1 expression by RNA interference in a target cell results in an attenuated HIV-1 replication and increases the amount of particulate CA cores in the cytosol of target cells. Furthermore, heat-inactivated, inhibitor-treated, or W34A/K63A Pin1 causes an attenuated *in vitro* uncoating of the HIV-1 core. The Pin1-dependent uncoating is inhibited by antisera raised against a CA peptide phosphorylated at Ser^{16} or treatment of the HIV-1 core with alkaline phosphatase. These findings provide insights into this obscure uncoating process in the HIV-1 life cycle and a new cellular target for HIV-1 drug development.

The HIV-1[4] CA protein must assemble properly and should be sufficiently stable to protect the genomic RNA but must disassemble to allow genomic RNA release after fusion. Because both the assembly and disassembly processes cannot act on the CA proteins at the same time, an important question concerns the mechanisms responsible for the switch from the assembly to disassembly mode. However, not much has been known about the disassembly process so far because this process has been assumed to occur immediately after fusion (1, 2).

Recent studies suggested that cell factors may assist the disassembly process, commonly referred to as uncoating (3, 4). Cellular activation has long been considered a requirement for HIV-1 infection of CD4$^+$ T cells, because HIV-1 fails to infect resting CD4$^+$ T cells from peripheral blood. Infection is aborted either during reverse transcription (5) or before nuclear import of the viral preintegration complex (6). It was shown that HIV-1 can enter resting CD4$^+$ T cells efficiently, but only short incomplete reverse transcripts are formed. Auewarakul *et al.* (3) demonstrated that the uncoating of HIV-1 is efficiently induced by lysate from activated CD4$^+$ lymphocytes, whereas resting CD4$^+$ lymphocyte lysate cannot uncoat the HIV-1 core. Furthermore, Warrilow *et al.* (4) reported that endogenous reverse transcription is inefficient in comparison with reverse transcription in cell infection, as exemplified by the poor efficiency of the production of intravirion late reverse transcription products. This observation also suggests a requirement for a contribution from the host cell environment for optimal HIV-1 reverse transcription to proceed by an ordered disassembly of the HIV-1 CA core. These findings suggest that the uncoating activity that releases the CA protein from the HIV-1 core is due to cellular factors.

We previously reported that the HIV-1 core is composed of some isoforms of the CA protein with different isoelectric points (7). The difference in isoelectric points among CA protein isoforms might be due to multiple post-translational modifications, such as phosphorylation. Indeed, several reports have provided evidence that the CA protein is predominantly phosphorylated at serine residues rather than threonine/tyrosine residues (8, 9). Phosphorylation often plays an important role in modulating protein activity and protein-protein interactions and promoting the disassembly of cellular macromolecular assembly such as the nuclear pore complex. Protein kinases catalyze post-translational phosphorylation, and many kinases are themselves regulated by phosphorylation. The phosphor-

* This work was supported in part by a Grant-in-Aid for Scientific Research from the Ministry of Education, Culture, Sports, Science, and Technology of Japan and a Health Science Research Grant from the Ministry of Health, Labour, and Welfare of Japan.

Author's Choice—Final version full access.

[S] The on-line version of this article (available at http://www.jbc.org) contains supplemental Table S1 and Figs. S1–S5.

[1] Both authors contributed equally to this work.

[2] To whom correspondence should be addressed: Kumamoto University, Dept. of Pharmaceutical Biochemistry, Faculty of Medical and Pharmaceutical Sciences, 5-1 Oe-Honmachi, Kumamoto 862-0973, Japan. Tel.: 81-96-371-4362; Fax: 81-96-362-7800; E-mail: misumi@gpo.kumamoto-u.ac.jp.

[3] Recipient of Japan Society for the Promotion of Science for Young Scientists Research Fellowship 217212.

[4] The abbreviations used are: HIV-1, human immunodeficiency virus type 1; CA, capsid; GST, glutathione *S*-transferase; CPE, cytopathic effect; ALP, alkaline phosphatase; RT, reverse transcriptase; PBS, phosphate-buffered saline; CBB, Coomassie Brilliant Blue; MALDI-TOF, matrix-assisted laser desorption ionization time-of-flight; KLH, keyhole limpet hemocyanin; ELISA, enzyme-linked immunosorbent assay; WT, wild type; mAb, monoclonal antibody; siRNA, small interfering RNA; RPDE, relative percentage of disassembly efficiency; MA, matrix; SIV, simian immunodeficiency virus.

ylation-dependent modulation of protein-protein interactions is the pivotal molecular switch for the regulation of signaling processes within eukaryotic cells. Furthermore, current studies point toward mitotic phosphorylation of nucleoporins as the trigger of the nuclear pore complex disassembly process (10–12). These findings led to a hypothesis that phosphorylation induces the dissociation of CA-CA protein interactions and promotes the disassembly of the HIV-1 core.

In this study, we show that the serine residue in the Ser^{16}-Pro^{17} motif of a CA protein isoform is phosphorylated and that peptidyl-prolyl isomerase Pin1 specifically recognizes the Ser^{16}-Pro^{17} motif of the HIV-1 core. Furthermore, we demonstrated that Pin1 prolyl isomerase activity is required for the disassembly of the HIV-1 core. These results reveal a novel regulation step of HIV-1 infection.

EXPERIMENTAL PROCEDURES

Virus Preparation—HIV-1_{LAV-1} and HIV-1_{JRFL} were prepared as previously described (7, 13). The supernatant from the culture medium of CEM/LAV-1 or CEM-CCR5/JRFL was filtered through a 0.22-μm-pore size disposable filter and then centrifuged at 43,000 × *g* for 3 h at 4 °C. The obtained pellet was resuspended in PBS(−) (0.02% KH_2PO_4, 0.29% $Na_2HPO_4 \cdot 12H_2O$, 0.8% NaCl, 0.02% KCl) and then centrifuged at 100,000 × *g* for 1 h at 4 °C. The resulting pellet was resuspended in 10 mM Tris-HCl buffer (pH 8.0). Virions were treated with or without 1 mg/ml subtilisin (ICN Biomedicals Inc., Costa Mesa, CA) in 10 mM Tris-HCl (pH 8.0) and 1 mM EDTA-2Na. The virions were then purified using PBS(−) by column chromatography with a 10-ml column of Sepharose CL-4B™ at room temperature in a biosafety hood. Fractions containing the virus were pooled and centrifuged at 100,000 × *g* for 1 h at 4 °C. The resulting pellet derived from HIV-1_{LAV-1} or HIV-1_{JRFL} was boiled for 1 min and lysed in 200 μl of lysis buffer (9.5 M urea, 2% (w/v) Nonidet P-40, 2% ampholine (pH 6–8), and 5% 2-mercaptoethanol). For the MAGIC-5 assay and quantitative analysis of HIV-1 reverse transcription, pNL4-3-based mutants and replication-defective viruses were prepared as follows. The HIV-1 proviral DNA constructs pNL4-3 (14), containing full-length HIV-1, and pNL4-3Δenv, in which there is a truncation in *env*, were the control viruses utilized in this study. The 1136-bp fragment containing the BssHII and SpeI sites of pNL4-3 or pNL4-3Δenv was subcloned into pT7Blue (Novagen, Inc., Madison, WI). Point mutations were introduced into the Ser^{16}-Pro^{17} motif in the HIV_{NL4-3} or $HIV_{NL4-3\Delta env}$ CA protein by site-directed mutagenesis. The fragments were sequenced to confirm mutations. The mutant BssHII-SpeI fragment was recloned into the full-length HIV expression plasmid pNL4-$3_{BssHII-SpeI}$ or pNL4-3$\Delta env_{BssHII-SpeI}$, which does not have the backbone BssHII-SpeI fragment. All of the mutations were verified by sequencing. The mutant viruses ($HIV_{NL4-3(S16A/P17A)}$, $HIV_{NL4-3\Delta envWT}$, and $HIV_{NL4-3\Delta env(S16A/P17A)}$) were produced by the transient transfection of HEK293 cells using pNL4-3(S16A/P17A) or pNL4-3Δenv and pNL4-3Δenv(S16A/P17A) with the pNL4-3-based env expression vector. Four days after transfection, the virus-containing supernatant was collected and clarified by filtration through 0.45-μm-pore size filters. Virus production and release were monitored by measuring virion-associated RT activity as previously described (7).

Peptide Mass Fingerprinting—An aliquot of the viral lysate was subjected to two-dimensional polyacrylamide gel electrophoresis in accordance with the method of O'Farrell (15). The sample was loaded using a 15-cm immobilized pH gradient tube gel (pH 6–8) (Daiichi Pure Chemicals Co., Ltd.). The proteins were focused for 1 h at 400 V followed by a step gradient (1000 V for 18 h; 2000 V for 1 h). After the second-dimensional run (10–20% PAG large gel; Daiichi Pure Chemicals Co., Ltd.), the gel was stained with Coomassie Brilliant Blue (CBB) R-250 or ProQ diamond (Invitrogen). CBB-stained gel pieces were excised from the gel and immersed in 100 μl of acetonitrile, dried under vacuum centrifugation, rehydrated in 25 μl of trypsin solution (3.9 ng/μl trypsin in 170 mM ammonium bicarbonate, 40% $H_2{}^{18}O$, 30% acetonitrile) or 25 μl of Glu-C solution (10 ng/μl Glu-C in 55 mM NaH_2PO_4 and 40% $H_2{}^{18}O$), and then incubated for 60 min. The unabsorbed enzyme solution was removed, and the gel pieces were incubated for 12 h at 37 °C. The digested peptides were purified using ZipTip (Nihon Millipore Ltd., Tokyo, Japan) and then analyzed by MALDI-TOF mass spectrometry as previously described (7). Phosphorylated peptides were analyzed as follows. Alkaline phosphatase (Wako Pure Chemical Industries, Ltd.) liberated the phosphate group from phosphorylated peptides. Alkaline phosphatase reactions were carried out directly on the MALDI target. The sample was mixed with 12 ng/ml ALP from *Escherichia coli* (Wako Pure Chemical Industries) that had been dissolved in 10 mM ammonium bicarbonate. The reactions were carried out for 5 min at room temperature followed by the addition of 0.5 μl of α-cyano-4-cinnamic acid or 2,5-dihydroxybenzoic acid saturated in 40% acetonitrile, 0.1% trifluoroacetic acid.

Preparation of HIV-1 p24-derived Peptide-Keyhole Limpet Hemocyanin (KLH) Conjugates and Antibody Screening—A p24-derived linear decapeptide (pSP, H_2N-HQAIpSPRTLN-COOH) was synthesized using an automatic peptide synthesizer. The molecular mass was determined by MALDI-TOF mass spectrometry (Burker Franzen Analytik). The amino group of His^1 was coupled to KLH (pSP-KLH) through bis(sulfosuccinimidyl)suberate (Thermo Fisher Scientific Inc.). Ten BALB/c mice were immunized intraperitoneally with 200 μg of pSP-KLH in Freund's adjuvant at 1-week intervals and administered an intravenous boost of 40 μg of pSP-KLH 3 days prior to splenectomy. The blood samples were collected prior to euthanasia and centrifuged at 1500 × *g* for 5 min, and the anti-pS16/P17 serum was harvested. Then the mice were euthanized, and their spleens were removed for *in vitro* hybridoma cell production. The hybridomas were generated by a standard method, by which splenocytes were fused with P3U1 cells and selected in hypoxanthine-, aminopterin-, and thymidine-supplemented media. In the screening, supernatants were tested for reactivity to ELISA plates coated with pSP. The hybridoma that produced high titers of anti-pS16/P17 mAb (3/D-6) was then cloned.

Preparation of HIV-1 CA Cores and Detection of Phosphorylated CA Protein in the HIV Core—The WT HIV CA cores were purified in accordance with the method of Auewarakul *et al.* (3) with some modifications. Briefly, 3 ml of purified cell-free viruses was overlayered on a discontinuous sucrose density gradient. The gradient was composed of 1 ml of 50% sucrose at the bottom and 1 ml of 10% sucrose containing 0.1% Igepal CA-630 on the top. The overlayered gradient was then centrifuged at 100,000 × *g* in a Swing Rotor P65ST (HitachiKoki Co., Ltd.) for 2 h at 4 °C. The pellets containing viral cores were then resuspended in the uncoating assay buffer (50 mM NaH_2PO_4, pH 7.2, 150 mM NaCl, and 200 μM sodium orthovanadate) and pooled. The CA cores were quantitated by measuring HIV-1 p24 antigen with RETRO-TEK HIV-1 p24 antigen ELISA (ZeptoMetrix Corp.). To examine the Ser^{16} phosphorylation of CA core, the pellets containing viral cores were then lysed with 62.5 mM Tris-HCl, 2% SDS, 10% glycerol (pH 6.8), and 10% 2-mercaptoethanol. The lysate from HIV cores was subjected to SDS-PAGE, and separated products were transferred to a polyvinylidene difluoride membrane for Western blotting. The membrane was stained with normal mouse serum and anti-pS16/P17 serum raised against pSP-KLH with or without pSP.

Viral Infectivity Assay—Jurkat and CEM cells (1 × 10^5) were exposed to the HEK293 cell-derived WT virus or S16A/P17A variant (100 ng of p24 antigen) for 2 h at 37 °C, washed with PBS(−), and cultured for 96 h. Virus infectivity was monitored by measurement of the p24 antigen from cell culture supernatants using RETRO-TEK HIV-1 p24 antigen ELISA (ZeptoMetrix Corp.).

Viral Entry Assay and Quantitative Analysis of HIV-1 Reverse Transcription during Acute Infection—The entry level of WT or mutant viruses was determined as follow. Viral entry assay was performed using the protocol of Kawano *et al.* (16) with modifications. MAGIC-5 cells (1 × 10^6 cells) were exposed to the virus (213.9 ng of HIV-1 RT) at 37 °C for 2 h. The cells were washed with PBS(−) and then incubated for 5 min at 37 °C in PBS(−) containing 0.25% trypsin. After trypsinization, the cells were washed twice with PBS(−) and pelleted. Cell-associated CA antigen content was determined by Western immunoblot analysis using an anti-p24 mAb (Immuno Diagnostics, Inc.). Furthermore, *de novo* synthesized HIV-1 cDNA was analyzed with or without Pin1 siRNA treatment in accordance with the method of Ikeda *et al.* (17).

Electron Microscopy of Virus—A viral preparation was fixed with 0.1 M sodium phosphate buffer (pH 7.4) containing 2% paraformaldehyde and 2.5% glutaraldehyde at 4 °C for 2 h prior to postfixation with 1% osmium tetroxide for 30 min at 4 °C. After dehydration in ethanol, the specimens were embedded in epoxy resin.

MAGIC-5 Assay and Cytopathic Effect (CPE) Assay—Viral infectivity was determined using MAGIC-5 cells as previously described in Ref. 18. MAGIC-5 cells (1 × 10^4 cells) were incubated in suspensions of WT, mutant, or single-round replication-defective viruses with 20 μg/ml DEAE dextran for 2 h and then cultured in a medium (200 μl) for 48 h. The cells were fixed, and HIV-1-infected cells identified by their blue staining were counted by conventional methods. To further examine whether a decrease in endogenous Pin1 expression level decreases viral infectivity, both MAGIC-5 assay and CPE assay were performed. 60 nM small interfering RNA against Pin1 (Pin1 C1 sense siRNA, GCCAUUUGAAGACGCCUCGdTdT; Pin1 C1 antisense siRNA, GAGGCGUCUUCAAAUGGC-dTdT; Pin1 C2 sense siRNA, CUGGCCUCACAGUUCAGCG-dTdT; Pin1 C2 antisense siRNA, CGCUGAACUGUGAGGC-CAGdTdT; Pin1 C3 sense siRNA, GCCGAGUGUAC-UACUUCAAdTdT; or Pin1 C3 antisense siRNA, UUGA-AGUAGUACACUCGGCdTdT) or control siRNA (sense siRNA against GL2 Luciferase, CGUACGCGGAAUACUUC-GAdTdT; or antisense siRNA, UCGAAGUAUUCCGCG-UACGdTdT) was transfected into the MAGIC-5 cells (1 × 10^4 or 2 × 10^5 cells) using Lipofectamine 2000. The cells were infected with HIV-1_{LAV-1} (12 ng of p24 antigen). HIV-1_{LAV-1}-infected cells identified by their blue staining were counted by conventional methods. In CPE assay, the cells were infected with a single-round replication-defective HIV-1 ($HIV_{NL4-3\Delta envWT}$, 11 ng of HIV RT).

Fate-of-Capsid Assay—Fate-of-capsid assay was performed in accordance with the method of Sodroski and co-workers (19) with some modifications. Briefly, recombinant HIV-1 virus-like particles (WT HIV-1(VSV-G) and S16A/P17A HIV-1(VSV-G)) were produced by cotransfection of 293T cells with pHCMV-G and pNL4-3Δenv or pNL4-3Δenv carrying the S16A/P17A mutation (pNL4-3Δenv(S16A/P17A)) as described in Ref. 20. To examine whether the infectivity defect of the S16A/P17A variant is linked to a dysfunction of uncoating, MAGIC-5 (4.5 × 10^6) cells were seeded in 60-cm^2 flasks and the next day incubated with either 5 ml of WT HIV-1(VSV-G) or 5 ml of S16A/P17A HIV-1(VSV-G) incubated at 37 °C for 4 h after 30 min of incubation at 4 °C. On the other hand, to examine whether Pin1 depletion is linked to a dysfunction of uncoating, MAGIC-5 cells (4.0 × 10^6) were transfected with Pin1 C1 and C2 siRNA (600 nM) or control siRNA (600 nM) using Neon™ transfection system (Invitrogen) and incubated for 44 h. The cells were further incubated with 5 ml of WT HIV-1(VSV-G) at 37 °C for 4 h after 30 min of incubation at 4 °C. These cells were washed three times with ice-cold PBS and detached by incubating with 2 ml of proteinase K (7 mg/ml in Dulbecco's modified Eagle's medium) for 5 min at 4 °C. The cells were washed once in Dulbecco's modified Eagle's medium containing 10% fetal bovine serum and twice in PBS. The pellets were resuspended in 2 ml of hypotonic lysis buffer (10 mM Tris-HCl, pH 8.0, 10 mM KCl, and 1 mM EDTA) and placed on ice for 15 min. The cells were lysed using a 7-ml Dounce homogenizer and 15 strokes with pestle B. Cell debris was removed by centrifugation for 3 min at 2,000 × *g*. After centrifugation, 1 ml of lysate was layered onto a 3.5-ml of 50% sucrose cushion (made in PBS) and centrifuged at 125,000 × *g* for 2 h at 4 °C in a Swing Rotor P65ST (HitachiKoki Co., Ltd). After centrifugation, 150 μl from the topmost part of the supernatant was collected and made 1× in SDS sample buffer. The pellets were resuspended in 10 μl of 1× SDS sample buffer. The samples were subjected to SDS-PAGE and Western blotting for CA proteins.

Determination of Pin1-CA Interaction—The interaction between Pin1 and the CA core was determined by GST-Pin1 pulldown assay. Recombinant Pin1 proteins were produced as N-terminal GST-tagged proteins as previously described (21). The CA core was treated with ALP (Wako Pure Chemical Industries) or heat-denatured ALP for 2 h (final concentration, 0.024 μg/μl ALP) in a buffer containing 50 mM NaH_2PO_4 (pH 7.2), 150 mM NaCl, 200 μM sodium orthovanadate, 10% glycerol, and 1% Triton X-100 and then incubated with 30 μl of beads containing GST or GST-Pin1 proteins for 2 h at 4 °C.

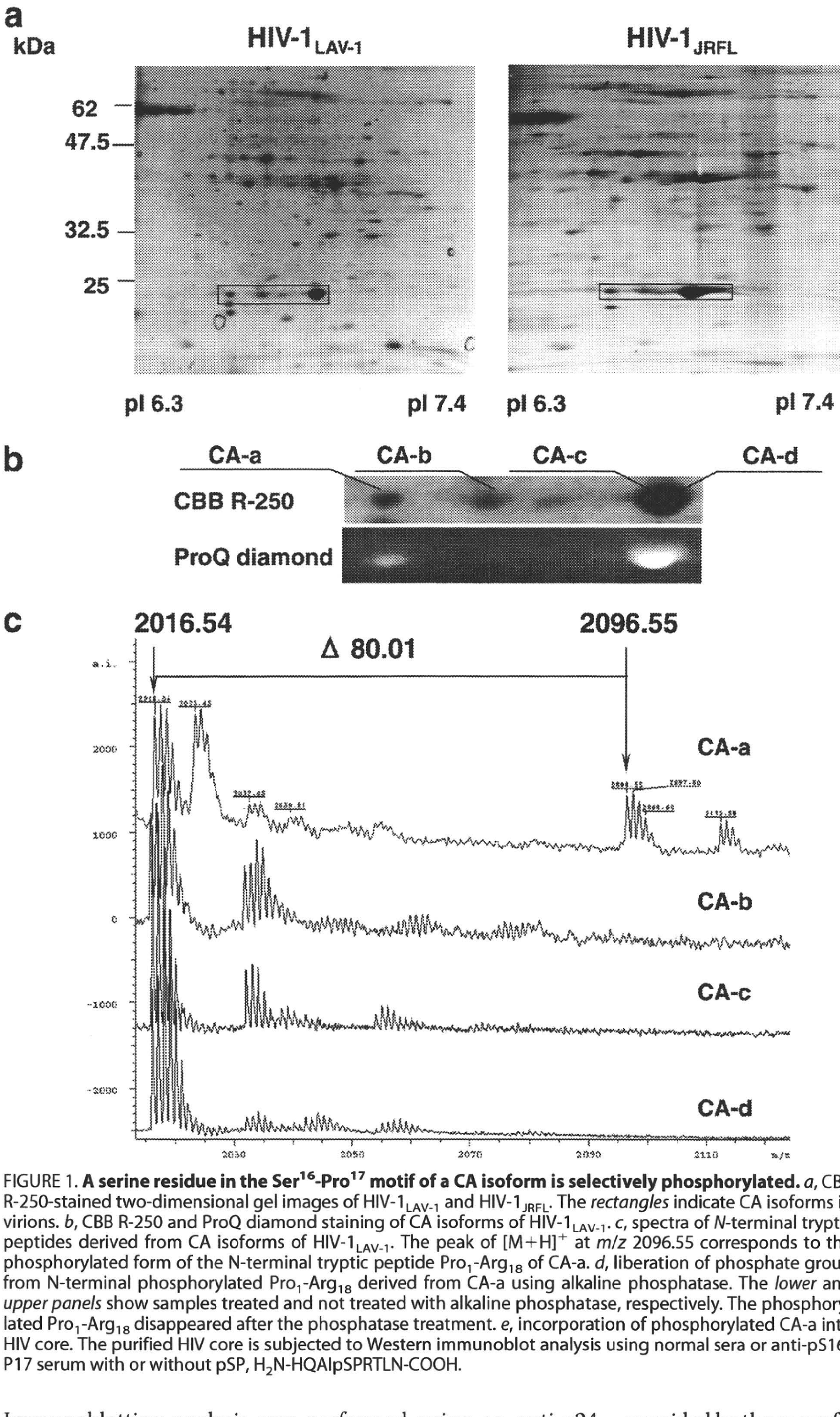

FIGURE 1. **A serine residue in the Ser^{16}-Pro^{17} motif of a CA isoform is selectively phosphorylated.** *a*, CBB R-250-stained two-dimensional gel images of HIV-1_{LAV-1} and HIV-1_{JRFL}. The *rectangles* indicate CA isoforms in virions. *b*, CBB R-250 and ProQ diamond staining of CA isoforms of HIV-1_{LAV-1}. *c*, spectra of *N*-terminal tryptic peptides derived from CA isoforms of HIV-1_{LAV-1}. The peak of $[M+H]^+$ at *m/z* 2096.55 corresponds to the phosphorylated form of the N-terminal tryptic peptide Pro_1-Arg_{18} of CA-a. *d*, liberation of phosphate group from N-terminal phosphorylated Pro_1-Arg_{18} derived from CA-a using alkaline phosphatase. The *lower* and *upper panels* show samples treated and not treated with alkaline phosphatase, respectively. The phosphorylated Pro_1-Arg_{18} disappeared after the phosphatase treatment. *e*, incorporation of phosphorylated CA-a into HIV core. The purified HIV core is subjected to Western immunoblot analysis using normal sera or anti-pS16/P17 serum with or without pSP, H_2N-HQAIpSPRTLN-COOH.

Immunoblotting analysis was performed using an anti-p24 mAb (Immuno Diagnostics, Inc.). Furthermore. a fraction of the ALP-treated CA core was subjected to Western blot analysis using an anti-pS16/P17 mAb raised against a synthetic phosphoserine-containing peptide, pSP, or an anti-p24 mAb.

Suppression of Pin1 Expression by siRNA—MAGIC-5 cells were transfected with Pin1 C3 siRNA (30–120 nM) or control siRNA (30–120 nM). The cells were infected with the WT virus and harvested 2 h after infection. To confirm the level of Pin1 expression, immunoblot analysis was carried out using the chemiluminescence protocol. The mouse monoclonal and goat polyclonal antibodies used were as follows: anti-Pin1 (R & D Systems, Inc.), anti-actin (Oncogene™ research product), and anti-lactate dehydrogenase (Chemicon) antibodies.

Uncoating Assay—The WT HIV CA core was purified as described above. The purified CA cores (2 ng) were resuspended in the uncoating assay buffer (50 mM NaH_2PO_4, pH 7.2, 150 mM NaCl, 200 μM sodium orthovanadate) and incubated with 0.114 μg/μl GST-Pin1, 0.114 μg/μl heat-denatured GST-Pin1, 0.114 μg/μl GST-Pin1 treated with juglone (molar ratio of GST-Pin1:juglone = 1:10; juglone was preincubated with GST-Pin1 at 37 °C for 1 h and then removed by gel filtration) or 0.114 μg/μl GST-Pin1(W34A/K63A) at 37 °C for 1 h. To examine whether the extent of CA disassembly was enhanced by Pin1, the pellets from the uncoating reactions were subjected to Western blot analysis using the anti-p24 mAb. Furthermore, a fraction of purified CA cores was pretreated with anti-pS16/P17 sera or normal sera. Another fraction of purified CA cores was treated with ALP (final concentration, 0.345 μg/μl) or heat-denatured ALP (final concentration, 0.345 μg/μl). The resulting CA cores were incubated with 0.114 μg/μl GST-Pin1 at 37 °C for 1 h. Each core suspension was then diluted in 5 ml of uncoating assay buffer and centrifuged at 100,000 × *g* for 2 h at 4 °C. The extent of CA release is quantified by p24 ELISA (ZeptoMetrix Corporation; the detection limit for the p24 antigen by ELISA was 7.8 pg/ml as provided by the manufacturer) because the undissociated cores were pelleted, and the dissociated CA protein was in the supernatant after ultracentrifugation. The relative percentage of disassembly efficiency (RPDE) is given by RPDE (%) = 100 × $(CA_S/CA_T)/(CA_{SC}/CA_{TC})$, where CA_S is the concentration of the CA protein in the supernatant, CA_T is the concentration of total CA protein in the supernatant plus pellet in the disassembly experiments of the CA core using boiled, juglone-treated

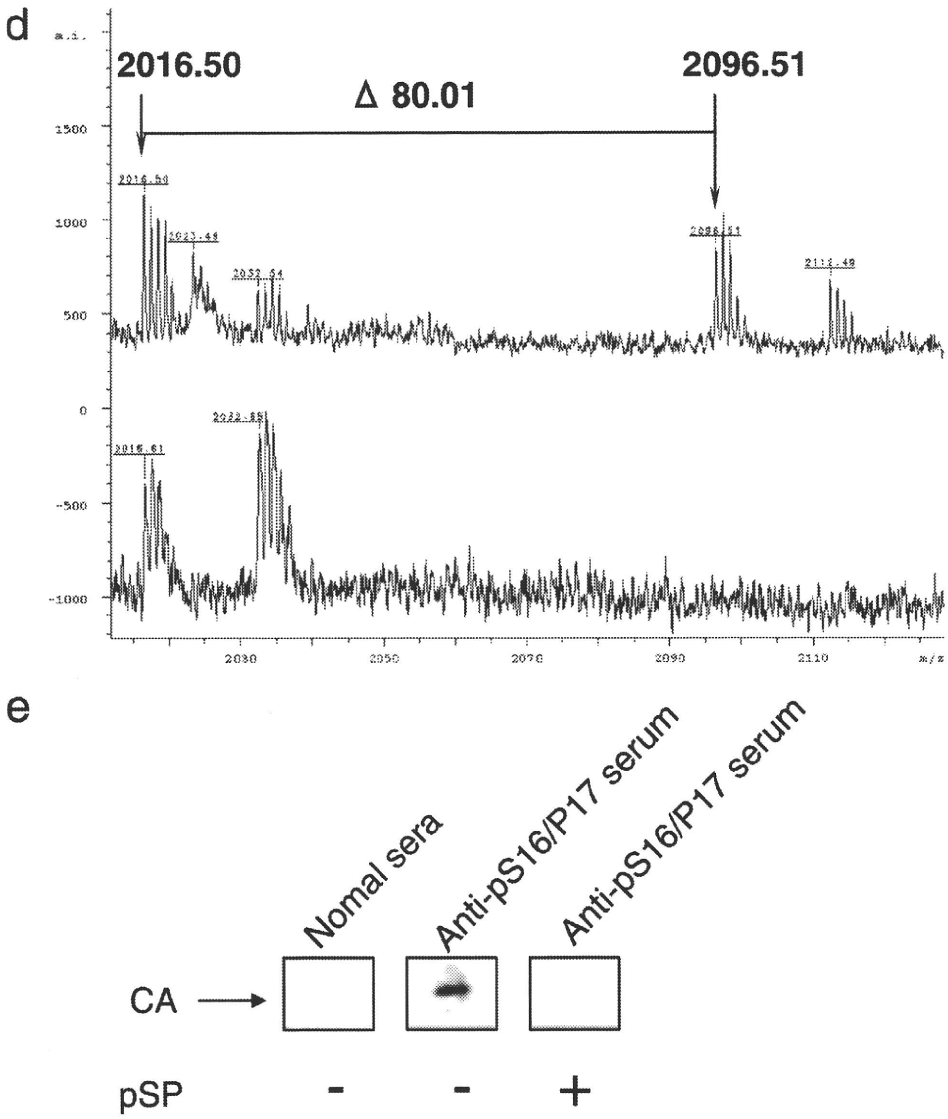

FIGURE 1—*continued*

identified by proteomics using two-dimensional gel electrophoresis and MALDI-TOF mass spectrometry (Fig. 1*a* and supplemental Table S1). We found that four isoforms of the HIV-1_{LAV-1} CA protein (CA-a (pI 6.70), CA-b (pI 6.80), CA-c (pI 6.91), and CA-d (pI 6.95)) are inside the virion (Fig. 1*b*). The differences between the pI values of the four isoforms of the CA protein may be due to post-translational modifications, such as phosphorylation and formylation (8, 9, 22, 23). Indeed, the CA proteins are composed of phosphorylated and unphosphorylated (Fig. 1*b*, *lower panel*) and formylated isoforms (23). Peptide mass fingerprinting data were used to identify the probable co/post-translational modifications. Then the specific phosphorylation of the N-terminal tryptic peptide (^{1}PIVQNIQGQMVHQAISPR^{18}) of CA-a was estimated because the spectrum corresponding to the N-terminal tryptic peptide exhibited a peak at m/z 2016.54 and the mass spectrum corresponding to the phosphorylated form exhibited a peak at m/z 2096.55 (Fig. 1*c*). The phosphorylation was confirmed by the liberation of a phosphate group from the N-terminal peptide of CA-a. The peak of $[M+H]^+$ at m/z 2016.50 corresponded to the peptide (^{1}PIVQNIQGQMVHQAISPR^{18}) whose phosphate group was cleaved off by an alkaline phosphatase (ALP) (Fig. 1*d*). These results show that the serine residue in the Ser^{16}-Pro^{17} motif of CA-a is selectively phosphorylated. To further determine whether CA-a is actually present in the CA core, the WT CA core was purified in accordance with the method of Auewarakul *et al.* (3) and was subjected to Western blot analysis using anti-pS16/P17 serum with or without pSP. As shown in Fig. 1*e*, CA-a is actually incorporated into the CA core.

GST-Pin1, or GST-Pin1(W34A/K63A); CA_{SC} is the concentration of the CA protein in the supernatant; and CA_{TC} is the concentration of total CA protein in the supernatant plus pellet in the control experiment using GST-Pin1. Likewise, the RPDE of CA cores pretreated with anti-pS16/P17 sera or ALP is given by RPDE (%) $= 100 \times (CA_S/CA_T)/(CA_{SC}/CA_{TC})$, where CA_S is the concentration of CA protein in the supernatant; CA_T is the concentration of total CA protein in the supernatant plus pellet in the disassembly experiments of CA core pretreated with anti-pS16/P17 sera or ALP using the GST-Pin1; CA_{SC} is the concentration of CA protein in the supernatant; and CA_{TC} is the concentration of total CA protein in the supernatant plus pellet in the control experiments of CA core pretreated with normal mouse sera or heat-denatured ALP using the GST-Pin1.

RESULTS

A CA Protein Isoform Is Selectively Phosphorylated at Serine Residue 16 in the Ser^{16}-Pro^{17} Motif and Incorporated into the HIV Core—Some isoforms of the HIV-1 CA protein associated with CXCR4-tropic HIV-1_{LAV-1} or CCR5-tropic HIV-1_{JRFL} were

Mutation at the Ser^{16}-Pro^{17} Motif Affects Uncoating Process—To study the role of the phosphorylated Ser^{16} that precedes Pro, we replaced Ser^{16} with glutamic acid (S16E) or alanine (S16A) to mimic phosphorylated or unphosphorylated Ser, respectively. We then tested the infectivity of the mutants by MAGIC-5 assay (21). The results showed that the S16E variant had the same infectivity as the wild type (Fig. 2*a*, *WT*). In contrast, the S16A variant had a decreased infectivity (Fig. 2*a*, $p < 0.01$). Assuming that glutamic acid mimics the negative charge of phosphorylated Ser^{16} in only a fraction of the CA protein in a viral core, the results obtained for S16E or S16A suggest that phosphorylation at Ser^{16} plays a critical role in maintaining

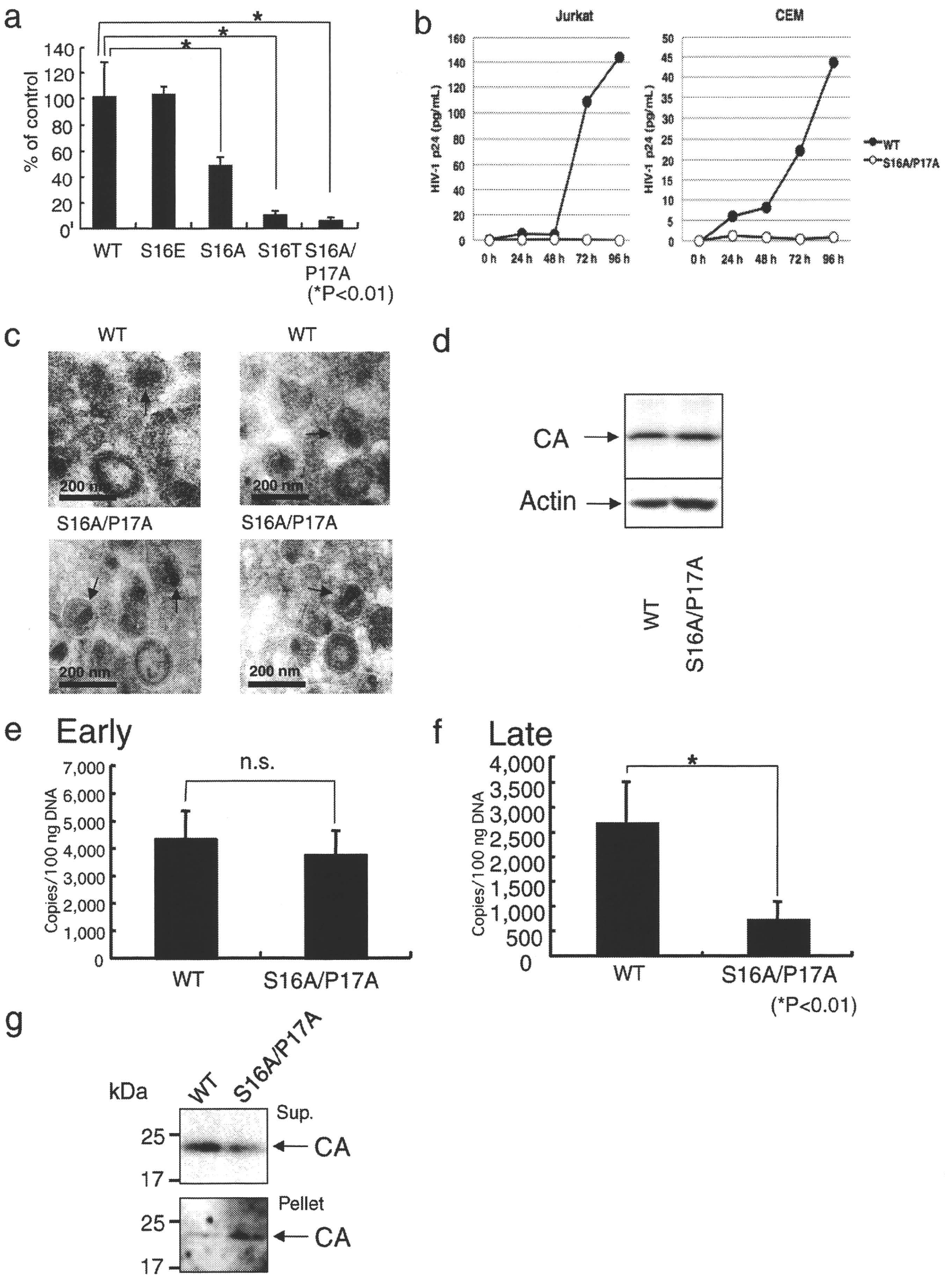
a
% of control
WT
S16E
S16A
S16T
S16A/P17A
(*P<0.01)
b
Jurkat
CEM
HIV-1 p24 (pg/mL)
WT
S16A/P17A
0 h 24 h 48 h 72 h 96 h
c
WT
S16A/P17A
200 nm
d
CA
Actin
WT
S16A/P17A
e
Early
n.s.
Copies/100 ng DNA
WT
S16A/P17A
f
Late
Copies/100 ng DNA
WT
S16A/P17A
(*P<0.01)
g
kDa
WT
S16A/P17A
Sup.
Pellet
CA
25
17

viral infectivity. To examine whether the phenotype of the S16A variant was specific to the selected amino acid changes, we produced another variant with a phosphorylatable amino acid residue, changing Ser to Thr (S16T). The S16T variant showed a remarkably decreased infectivity compared with the WT virus (Fig. 2*a*, $p < 0.01$), suggesting that the Ser^{16} residue in the highly conserved Ser^{16}-Pro^{17} motif (supplemental Fig. S1) plays an important role in maintaining the viral infectivity. To further investigate why Ser^{16} in a fraction of the CA protein in the virion needs to be phosphorylated, we generated another variant (S16A/P17A) because single-point mutations of Ser^{16} in the Ser^{16}-Pro^{17} motif may provide an alternate binding site for conventional peptidyl-prolyl *cis-trans* isomerases, such as cyclophilins, or FK-506-binding proteins, which catalyze the *cis-trans* isomerization of Xaa-Pro peptide bonds (where Xaa is the preceding amino acid) in oligopeptides or proteins. The S16A/P17A variant also had a markedly decreased infectivity in MAGIC-5 cells (Fig. 2*a*, $p < 0.01$) and could not replicate efficiently in T cell lines, Jurkat cells, and CEM cells (Fig. 2*b*), although the core yield of the S16A/P17A variant from HEK293 cells was very similar to that of WT HIV-1, and the phenotypes of the CA core were normal (Fig. 2*c*). Furthermore, to determine whether the lack of infectivity of S16A/P17A was due to a defect in the reverse transcription process, we carried out a viral entry assay and quantitative real time PCR analysis using primers designed to specifically amplify early or late products of reverse transcription. The viral entry assay indicated that the entry levels of S16A/P17A and WT were the same because the amounts of S16A/P17A CA protein in subcellular fractions were very similar to that of WT CA protein (Fig. 2*d*). However, compared with WT, S16A/P17A produced the same level of the early (R/U5) form of the viral cDNA product (Fig. 2*e*) but showed a significant decrease in the level of the late (R/gag) form of the viral cDNA product (Fig. 2*f*, $p < 0.01$). To further examine whether the infectivity defect of the S16A/P17A variant is linked to a dysfunction of uncoating, cell-based fate-of-capsid uncoating assay developed by Sodroski's group (19) was performed. This assay allows us to measure the amounts of cores and soluble free forms of the CA protein present in the cytosol of infected cells. Moreover, the appearance of CA cores in the cytosol inversely correlates with the proper conversion of CA cores to soluble CA in target cells. The amounts of pelletable CA cores in the cells infected with the S16A/P17A mutant virus increased against those detected in the cells infected with WT virus (Fig. 2*g*, *lower panel*, *Pellet*). Furthermore, the levels of the CA protein in the supernatants from MAGIC-5 cells incubated with the S16A/P17A mutant virus were lower than those detected in the cells infected with WT virus (Fig. 2*g*, *upper panel*, *Sup.*). These results suggest that the infectivity defect of the S16A/P17A variant is linked to a dysfunction of the uncoating process.

Pin1 within the Target Cell Affects an Early Phase in HIV-1 Replication—Pin1 is a peptidyl-prolyl isomerase that specifically recognizes phosphorylated serine/threonine followed by proline via its WW domain and then catalyzes a conformational change of the bound substrate in a phosphorylation-dependent manner (24, 25). Pin1 has been shown to regulate the stability and localization of its substrates during transcriptional activation, cell cycle progression, and cell death, and a deregulated expression or loss of function of Pin1 leads to the progression of serious human diseases such as cancer and Alzheimer disease (24, 26–28). We therefore considered that Pin1 might bind to and regulate the function of the CA core. We first investigated whether Pin1 directly binds to the CA core by GST-Pin1 pull-down assay. Glutathione beads containing GST or GST-Pin1 were incubated with the CA core purified in accordance with the method described under "Experimental Procedures." To demonstrate that cores were indeed successfully purified, we performed a comparative immunoblot analysis of core preparations. As expected, the membrane-associated matrix (MA) protein (supplemental Fig. S2*a*) and the HIV surface glycoprotein gp120 (supplemental Fig. S2*b*) were substantially depleted in the core preparation. These results indicated that CA core is sufficiently purified. Therefore, in Pin1 pulldown assay, the binding proteins were then analyzed by immunoblotting with an anti-CA antibody. Fig. 3*a* shows that GST-Pin1, but not GST, was bound to the CA core. To investigate whether the binding of the CA core is directly due to the phosphorylation of Ser^{16} in the CA core, WT core particles were treated with ALP or the heat-denatured ALP. The treatment removed phosphate groups from phosphorylated Ser^{16} (Fig. 3*b*) and eliminated the Pin1 binding activity of the CA core (Fig. 3*c*). There are three highly conserved Ser-Pro motifs (Ser^{16}-Pro^{17}, Ser^{33}-Pro^{34}, and Ser^{146}-Pro^{147}) and a conserved Thr^{48}-Pro^{49} motif in the CA protein (supplemental Fig. S1). To examine whether Ser^{33}, Thr^{48}, or Ser^{146} in CA core is phosphorylated, the mixture of CA protein isoforms were subjected to proteome analysis (supplemental Fig. S3). The data demonstrated that Ser^{33}, Thr^{48}, and Ser^{146} in CA core were not phosphorylated. These results suggested that Pin1 binds preferentially to the phosphorylated Ser^{16}-Pro^{17} motif.

Because Pin1 has CA core binding activity, we next determined whether a decrease in endogenous Pin1 expression level decreases HIV-1 infectivity. We transfected MAGIC-5 cells

FIGURE 2. **The S16A/P17A CA mutant shows impaired uncoating process.** *a*, effect of various mutations in Ser^{16}-Pro^{17} motif on viral infectivity. Viral infectivity was determined using MAGIC-5 cells as previously described in Ref. 18. MAGIC-5 cells (1×10^4 cells) were exposed to an equal amount of WT or mutant viruses (corresponding to 3 ng RT). Statistical analysis using the analysis of variance test was performed. The *error bars* denote the standard deviation. *b*, replication kinetics of S16A/P17A variant in Jurkat and CEM cells. *c*, effect of alanine mutation of Ser^{16}-Pro^{17} motif on viral core phenotype. The *arrows* indicate electron-dense cores typical of intact HIV. *d*, effect of alanine mutation of Ser^{16}-Pro^{17} motif on viral entry efficiency. Viral entry assay was performed as described under "Experimental Procedures." *e* and *f*, quantitative analysis of HIV-1 reverse transcription during acute infection using early stage primers (*e*, R/U5) and late stage primers (*f*, R/gag). Briefly, MAGIC-5 cells (1×10^6 cells) were exposed to WT or S16A/P17A virus (2.5 ng of HIV-1 RT) and harvested at 1 day postinfection. The cells were washed with PBS(−), and nucleic acids were extracted. Quantitative analysis was performed using the same primers in accordance with the method of Ikeda *et al.* (17). The significant differences (unpaired *t* test) are indicated as follows: *, $p < 0.01$; *n.s.*, not significant. The *error bars* denote the standard deviation. *g*, effect of Ser^{16}-Pro^{17} motif on fate of CA core in infected cells. MAGIC-5 cells were incubated with WT HIV-1(VSV-G) or S16A/P17A HIV-1(VSV-G) at 4 °C for 30 min and then at 37 °C for 4 h. The cell lysates were analyzed as described under "Experimental Procedures." The supernatants and pellets were Western blotted for CA proteins.

with siRNA against Pin1 or control siRNA. As shown in the *top panel* of Fig. 3*d*, Pin1 siRNA (Pin1 C3) specifically decreased the Pin1 expression level in MAGIC-5 cells without altering actin or lactate dehydrogenase expression level. The cells were infected with HIV-1_{LAV-1}, and β-galactosidase activity was measured as an indicator of infection. In Fig. 3*e*, 60 nM Pin1 siRNA (Pin1 C3)-treated MAGIC-5 cells were infected with HIV-1_{LAV-1} (12 ng of p24 antigen) under the condition in which no HIV-1_{LAV-1}-induced CPE was observed in 60 nM control siRNA-treated MAGIC-5 cells. Interestingly, a decrease in endogenous Pin1 expression level decreased HIV-1_{LAV-1} infectivity (Fig. 3*e*, $p < 0.01$). Furthermore, the effects of Pin1-targeted siRNA treatment on HIV-1 replication were evaluated on the basis of cytopathic effect (*y*) observations (Fig. 3, *f–i*) and quantitative real time PCR analysis using primers designed to specifically amplify late products of reverse transcription. 60 nM

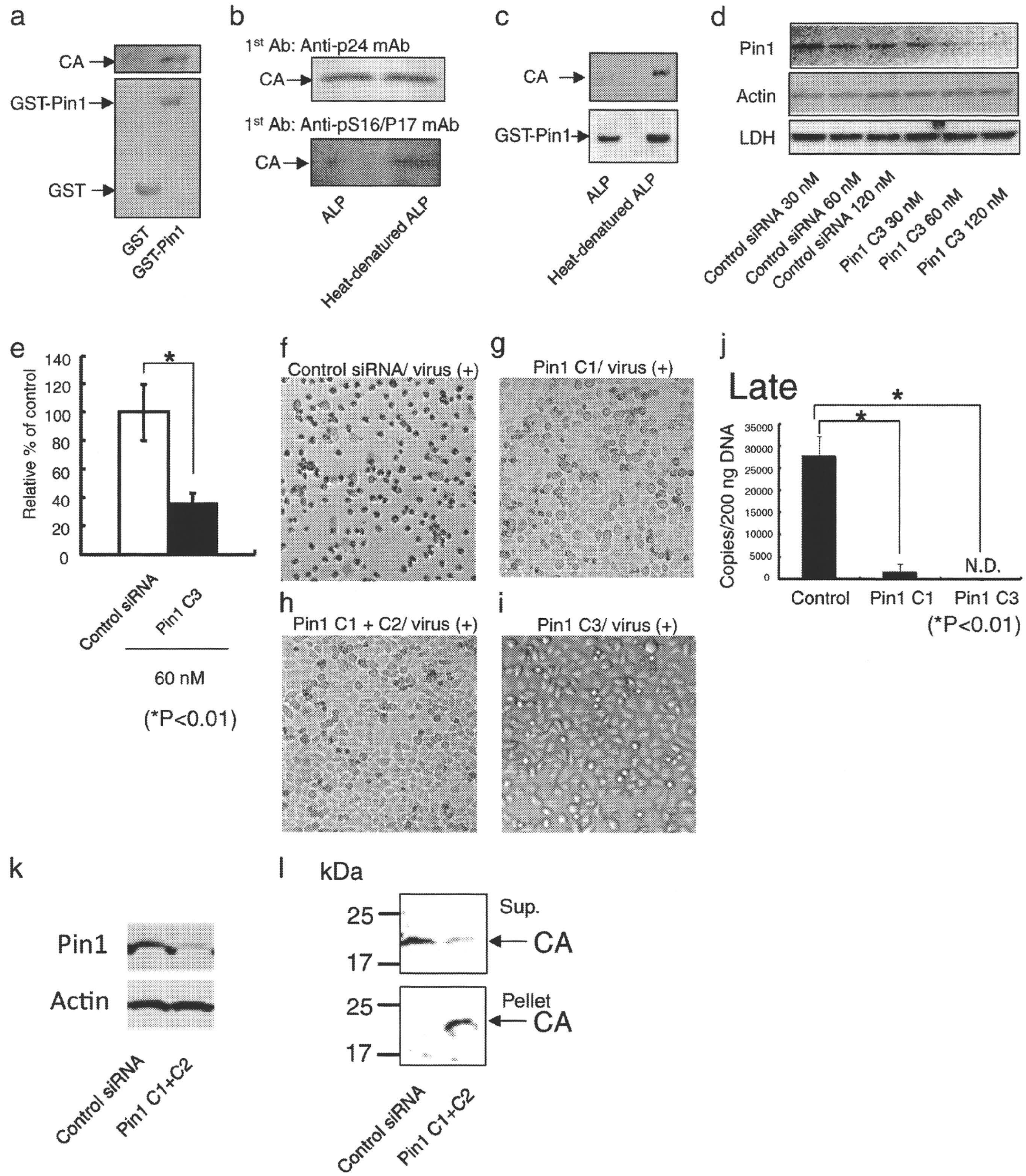

Pin1 C1-, C1+C2-, or C3-treated MAGIC-5 cells was infected with a single-round replication-defective HIV-1 under the condition in which a single-round replication-defective HIV-1-induced CPE was observed in 60 nM control siRNA-treated MAGIC-5 cells (Fig. 3, *f–i*). After treatment with siRNAs, MAGIC-5 cells were infected with single-round replication-defective $HIV_{NL4-3\Delta envWT}$ (11 ng of HIV RT). CPE in infected cells treated with the control siRNA was observed at 46 h postinfection (Fig. 3*f*). On the other hand, CPE was hardly observed in cells treated with 60 nM Pin1 C1, C1+C2, or C3 (Fig. 3, *g–i*, respectively). This indicates that Pin1-targeted siRNAs are capable of inhibiting CPE induced by HIV infection. Furthermore, Fig. 3*j* shows that there was a significant decrease in the level of the late (R/gag) form of the viral cDNA product.

To further examine whether Pin1 depletion is linked to a dysfunction of uncoating, cell-based fate-of-capsid uncoating assay was performed. The amounts of pelletable CA cores in the Pin1 knockdown cells infected with WT HIV-1(VSV-G) increased against those detected in the control siRNA-treated cells infected with WT HIV-1(VSV-G) (Fig. 3, *k* and *l*, *lower panels*, *Pellet*). Furthermore, the levels of the CA protein in the supernatants from the Pin1 knockdown cells infected with WT HIV-1(VSV-G) were lower than those detected in the control siRNA-treated cells infected with the WT HIV-1(VSV-G) (Fig. 3*l*, *upper panel*, *Sup.*). These results indicate that Pin1 depletion is linked to a dysfunction of uncoating.

Pin1 Induces Disassembly of the CA Core—Pin1 might regulate the uncoating of the CA core. To test this possibility, we attempted to study this process *in vitro* by detecting the disassembly of the CA core in the presence of Pin1. Purified CA cores were diluted with an uncoating assay buffer and incubated with GST-Pin1, heat-denatured, inhibitor-treated, or W34A/K63A GST-Pin1. Following incubation, the CA cores were subjected to ultracentrifugation to separate the free CA protein from the intact CA core. CA core dissociation was found to be GST-Pin1-dependent (Fig. 4*a*, *lane 2*), and the effect was attenuated when Pin1 was denatured (Fig. 4*b*, $p < 0.01$) or treated with the Pin1 inhibitor juglone (Fig. 4*c*, $p < 0.01$) and catalytically inactived the W34A/K63A Pin1 mutant (Fig. 4*d*, $p < 0.01$). Furthermore, the uncoating assay demonstrated that the Pin1-dependent disassembly was competed with the anti-pS16/P17 serum (Fig. 4*e*, $p < 0.01$) and blocked by the pretreatment of the core with ALP (Fig. 4*e*, $p < 0.01$). These results support the idea that Pin1 facilitates the HIV-1 uncoating by interacting with the CA core.

DISCUSSION

Much is known about the structure of the HIV-1 CA protein (29–31), but the mechanism and requirement of HIV-1 uncoating in postentry events have remained poorly defined. However, recent studies showed that the HIV-1 uncoating activity, which releases the CA protein from HIV-1 cores and is required for the activation of reverse transcriptase, is due to cellular factors (3, 4). The studies suggest that the ordered uncoating process of HIV-1 is not spontaneous and is regulated by cellular factors. Therefore, we employed a series of biochemical approaches to clarify the mechanism of HIV-1 CA core uncoating.

In this study, we showed that Pin1 assists the uncoating of the HIV core. Proteome analysis suggests that the Ser residue in the Ser^{16}-Pro^{17} motif of CA-a is preferentially phosphorylated (Fig. 1, *c* and *d*). Interestingly, three Ser-Pro motifs (Ser^{16}-Pro^{17}, Ser^{33}-Pro^{34}, and Ser^{146}-Pro^{147}) are highly conserved across HIV-1 clades (supplemental Fig. S1), and only the Ser^{16}-Pro^{17} motif is conserved among HIV-1, HIV-2, and simian immunodeficiency virus (SIV) (supplemental Fig. S4). As shown in Figs. 2*g* and 3*l*, cell-based fate-of-capsid uncoating assay demonstrated that the infectivity defect of the S16A/P17A variant is linked to a dysfunction of the uncoating process, and Pin1 depletion in the target cells is linked to a dysfunction of uncoating. Furthermore, GST-Pin1 pulldown assay and *in vitro* uncoating assay indicated that Pin1 facilitates HIV-1 uncoating by interacting with the CA core through the Ser^{16}-Pro^{17} motif (Figs. 3, *b* and *c*, and 4, *e* and *f*). These results suggest that only a fraction of the CA protein phosphorylated at Ser^{16}-Pro^{17} motif serves as a molecular switch to signal CA core uncoating because both the assembly and disassembly pathways cannot act on the CA core at the same time.

To investigate how the motif of CA-a is phosphorylated, Western immunoblot analysis with monoclonal anti-pS16/P17 mAb was carried out, which demonstrated that Ser^{16} was phosphorylated inside $HIV\text{-}1_{LAV\text{-}1}$ virions but not inside CEM/LAV-1 cells, although the specific kinase that phosphorylates Ser^{16} is currently unknown (supplemental Fig. S5). As shown in Fig. 3*e*, a decrease in endogenous Pin1 expression level decreases HIV-1 infectivity. These findings suggest that the CA

FIGURE 3. **Interactions of Pin1 with the CA core and Pin1 within the target cells regulate HIV-1 infectivity.** *a*, the CA core was subjected to GST-Pin1 pulldown assay and immunoblotted with anti-p24 mAb (*upper panel*). CBB staining of GST and GST-Pin1 (*lower panel*). *b*, treatment of CA core with ALP or heat-denatured ALP. The ALP- and heat-denatured ALP-treated CA cores were subjected to Western immunoblot analysis using anti-pS16/P17 mAb or anti-p24 mAb. The treatment removed phosphate groups from phosphorylated Ser^{16}. *c*, effect of ALP on interaction between Pin and CA core. The ALP-treated CA core was subjected to GST-Pin1 pulldown assay and immunoblotted with anti-p24 mAb (*upper panel*). CBB staining of GST-Pin1 is shown (*lower panel*). *d* and *e*, the suppression of Pin1 expression by 60 nM Pin1 C3 siRNA (*d*, *upper panel*, the expressions of actin and lactate dehydrogenase (*LDH*) were not affected by Pin1-specific siRNA)) in MAGIC-5 cells (1×10^4 cells) results in an attenuated $HIV\text{-}1_{LAV\text{-}1}$ replication (*e*). The significant differences (unpaired *t* test) are indicated as follows: *, $p < 0.01$. The *error bars* denote the standard deviation. *f–i*, the effects of Pin1-specific siRNAs were evaluated on the basis of CPE observations. The cells (2×10^5 cells) were pretreated with 60 nM control siRNA (*f*), Pin1 C1 (*g*), Pin1 C1+C2 (*h*), and Pin1 C3 (*i*) and then infected with single-round replication-defective HIV-1 ($HIV_{NL4-3\Delta envWT}$). Pin1-specific siRNAs were capable of inhibiting CPE induced by HIV infection. *j*, effect of Pin1 siRNAs on reverse transcription. The knockdown of Pin1 showed that there was a significant decrease in the level of the late (R/gag) form of the viral cDNA product. Statistical analysis using the analysis of variance test was performed. The *error bars* denote the standard deviation. *N.D.*, not detected. The detection limit of late products of HIV-1 reverse transcription was 400 copies/reaction in the assay. *k*, Pin1 C1+C2-induced suppression of Pin1 expression. MAGIC-5 cells were transfected with Pin1 C1+C2 siRNA (600 nM) using the Neon™ transfection system (*upper panel*, the expression of actin was not affected by Pin1 C1+C2). *l*, effect of Pin1 depletion on fate of CA core in infected cells. Pin1 knockdown cells treated with Pin1 C1+C2 siRNA were incubated with WT HIV-1(VSV-G) at 4 °C for 30 min and then at 37 °C for 4 h. The cell lysates were analyzed as described under "Experimental Procedures." The supernatants and pellets were analyzed by Western blotting for the CA proteins.

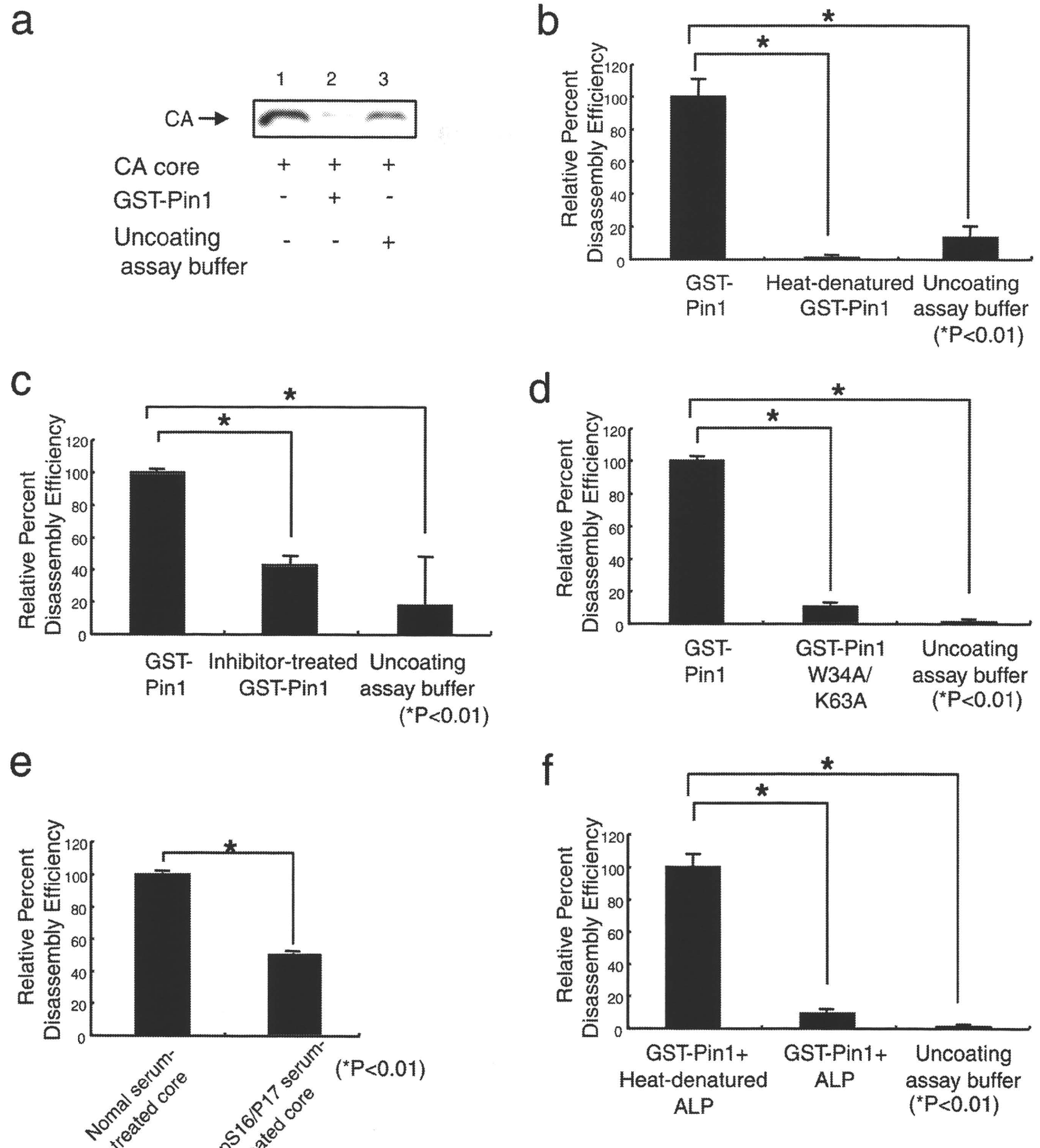

FIGURE 4. ***In vitro* uncoating of CA core by GST-Pin1.** *a*, *in vitro* uncoating assay was performed as described under "Experimental Procedures." The extent of uncoating was visualized by Western blot analysis using anti-p24 mAb after the undisassembled cores have been pelleted in an ultracentrifuge. CA cores in the presence of GST-Pin1 disassembled *in vitro* (*lane 2*). The quantities of the CA protein in the pellets in the presence of uncoating assay buffer were similar to that of the input CA protein (*lanes 1* and *3*). *b*, after incubating HIV-1 cores with GST-Pin1, heat-denatured GST-Pin1, or uncoating assay buffer for 1 h, the relative percentage of disassembly efficiency is given by the equation shown under "Experimental Procedures." Pin1 induces disassembly of the CA cores. *c*, *in vitro* uncoating activities after incubating HIV-1 cores with juglone-treated Pin1 for 1 h. The treatment of GST-Pin1 with juglone results in an attenuated *in vitro* uncoating. *d*, effect of GST-Pin1 (W34A/K63A) on uncoating. *In vitro* uncoating activities after incubating GST-Pin1 (W34A/K63A) with CA cores for 1 h. *e*, *in vitro* competitive uncoating assay. The pretreatment of CA cores with anti-pS16/p17 serum results in an attenuated *in vitro* uncoating. *f*, *in vitro* uncoating activities after incubating HIV CA cores with ALP for 2 h. Pin1-dependent disassembly was blocked by the pretreatment of the cores with ALP. *b–f*, statistical analysis using the analysis of variance test was performed. The *error bars* denote the standard deviation. The significant differences are indicated as follows: *, $p < 0.01$.

core phosphorylated inside the viral particle after release from the infected cells associates directly with Pin1 after entry into host cells for the uncoating process. A better understanding of these findings is crucial not only for elucidating the uncoating process at the early stage of the HIV-1 life cycle but also for identifying new anti-HIV drugs.

Acknowledgments—We thank A. Muneoka (Shin Nippon Biomedical Laboratories, Ltd.) for the technical support during electron microscopy. We thank Dr. R. Swanstrom (Lineberger Comprehensive Cancer Center, University of North Carolina at Chapel Hill) for support in preparing pNL4-3Δenv(S16A/P17A) with the pNL4-3-based env expression vector and helpful discussions.

REFERENCES

1. Goff, S. P. (2001) *J. Gene Med.* **3,** 517–528
2. Dvorin, J. D., and Malim, M. H. (2003) *Curr. Top. Microbiol. Immunol.* **281,** 179–208
3. Auewarakul, P., Wacharapornin, P., Srichatrapimuk, S., Chutipongtanate, S., and Puthavathana, P. (2005) *Virology* **337,** 93–101
4. Warrilow, D., Meredith, L., Davis, A., Burrell, C., Li, P., and Harrich, D. (2008) *J. Virol.* **82,** 1425–1437
5. Zack, J. A., Arrigo, S. J., Weitsman, S. R., Go, A. S., Haislip, A., and Chen, I. S. (1990) *Cell* **61,** 213–222
6. Stevenson, M., Stanwick, T. L., Dempsey, M. P., and Lamonica, C. A. (1990) *EMBO J.* **9,** 1551–1560
7. Misumi, S., Fuchigami, T., Takamune, N., Takahashi, I., Takama, M., and Shoji, S. (2002) *J. Virol.* **76,** 10000–10008
8. Veronese, F. D., Copeland, T. D., Oroszlan, S., Gallo, R. C., and Sarngadharan, M. G. (1988) *J. Virol.* **62,** 795–801
9. Mervis, R. J., Ahmad, N., Lillehoj, E. P., Raum, M. G., Salazar, F. H., Chan, H. W., and Venkatesan, S. (1988) *J. Virol.* **62,** 3993–4002
10. Macaulay, C., Meier, E., and Forbes, D. J. (1995) *J. Biol. Chem.* **270,** 254–262
11. Favreau, C., Worman, H. J., Wozniak, R. W., Frappier, T., and Courvalin, J. C. (1996) *Biochemistry* **35,** 8035–8044
12. Glavy, J. S., Krutchinsky, A. N., Cristea, I. M., Berke, I. C., Boehmer, T., Blobel, G., and Chait, B. T. (2007) *Proc. Natl. Acad. Sci. U.S.A.* **104,** 3811–3816
13. Ott, D. E., Coren, L. V., Kane, B. P., Busch, L. K., Johnson, D. G., Sowder, R. C., 2nd, Chertova, E. N., Arthur, L. O., and Henderson, L. E. (1996) *J. Virol.* **70,** 7734–7743
14. Adachi, A., Gendelman, H. E., Koenig, S., Folks, T., Willey, R., Rabson, A., and Martin, M. A. (1986) *J. Virol.* **59,** 284–291
15. O'Farrell, P. H. (1975) *J. Biol. Chem.* **250,** 4007–4021
16. Kawano, Y., Tanaka, Y., Misawa, N., Tanaka, R., Kira, J. I., Kimura, T., Fukushi, M., Sano, K., Goto, T., Nakai, M., Kobayashi, T., Yamamoto, N., and Koyanagi, Y. (1997) *J. Virol.* **71,** 8456–8466
17. Ikeda, T., Nishitsuji, H., Zhou, X., Nara, N., Ohashi, T., Kannagi, M., and Masuda, T. (2004) *J. Virol.* **78,** 11563–11573
18. Hachiya, A., Aizawa-Matsuoka, S., Tanaka, M., Takahashi, Y., Ida, S., Gatanaga, H., Hirabayashi, Y., Kojima, A., Tatsumi, M., and Oka, S. (2001) *Antimicrob. Agents Chemother.* **45,** 495–501
19. Stremlau, M., Perron, M., Lee, M., Li, Y., Song, B., Javanbakht, H., Diaz-Griffero, F., Anderson, D. J., Sundquist, W. I., and Sodroski, J. (2006) *Proc. Natl. Acad. Sci. U.S.A.* **103,** 5514–5519
20. Yee, J. K., Miyanohara, A., LaPorte, P., Bouic, K., Burns, J. C., and Friedmann, T. (1994) *Proc. Natl. Acad. Sci. U.S.A.* **91,** 9564–9568
21. Shen, M., Stukenberg, P. T., Kirschner, M. W., and Lu, K. P. (1998) *Genes Dev.* **12,** 706–720
22. Laurent, A. G., Krust, B., Rey, M. A., Montagnier, L., and Hovanessian, A. G. (1989) *J. Virol.* **63,** 4074–4078
23. Fuchigami, T., Misumi, S., Takamune, N., Takahashi, I., Takama, M., and Shoji, S. (2002) *Biochem. Biophys. Res. Commun.* **293,** 1107–1113
24. Wulf, G., Finn, G., Suizu, F., and Lu, K. P. (2005) *Nat. Cell Biol.* **7,** 435–441
25. Lu, K. P., Hanes, S. D., and Hunter, T. (1996) *Nature* **380,** 544–547
26. Ryo, A., Nakamura, M., Wulf, G., Liou, Y. C., and Lu, K. P. (2001) *Nat. Cell Biol.* **3,** 793–801
27. Zacchi, P., Gostissa, M., Uchida, T., Salvagno, C., Avolio, F., Volinia, S., Ronai, Z., Blandino, G., Schneider, C., and Del Sal, G. (2002) *Nature* **419,** 853–857
28. Liou, Y. C., Sun, A., Ryo, A., Zhou, X. Z., Yu, Z. X., Huang, H. K., Uchida, T., Bronson, R., Bing, G., Li, X., Hunter, T., and Lu, K. P. (2003) *Nature* **424,** 556–561
29. Gamble, T. R., Vajdos, F. F., Yoo, S., Worthylake, D. K., Houseweart, M., Sundquist, W. I., and Hill, C. P. (1996) *Cell* **87,** 1285–1294
30. Gamble, T. R., Yoo, S., Vajdos, F. F., von Schwedler, U. K., Worthylake, D. K., Wang, H., McCutcheon, J. P., Sundquist, W. I., and Hill, C. P. (1997) *Science* **278,** 849–853
31. Gitti, R. K., Lee, B. M., Walker, J., Summers, M. F., Yoo, S., and Sundquist, W. I. (1996) *Science* **273,** 231–235